

University of Windsor

Scholarship at UWindor

Electronic Theses and Dissertations

Theses, Dissertations, and Major Papers

7-2-2018

MODELING AND SIMULATION OF PM MOTOR TESTING ENVIRONMENT TOWARDS EV APPLICATION CONSIDERING ROAD CONDITIONS

Qingqing Xie
University of Windsor

Follow this and additional works at: <https://scholar.uwindsor.ca/etd>

Recommended Citation

Xie, Qingqing, "MODELING AND SIMULATION OF PM MOTOR TESTING ENVIRONMENT TOWARDS EV APPLICATION CONSIDERING ROAD CONDITIONS" (2018). *Electronic Theses and Dissertations*. 7485. <https://scholar.uwindsor.ca/etd/7485>

This online database contains the full-text of PhD dissertations and Masters' theses of University of Windsor students from 1954 forward. These documents are made available for personal study and research purposes only, in accordance with the Canadian Copyright Act and the Creative Commons license—CC BY-NC-ND (Attribution, Non-Commercial, No Derivative Works). Under this license, works must always be attributed to the copyright holder (original author), cannot be used for any commercial purposes, and may not be altered. Any other use would require the permission of the copyright holder. Students may inquire about withdrawing their dissertation and/or thesis from this database. For additional inquiries, please contact the repository administrator via email (scholarship@uwindsor.ca) or by telephone at 519-253-3000ext. 3208.

**MODELING AND SIMULATION OF PM MOTOR
TESTING ENVIRONMENT TOWARDS EV
APPLICATION CONSIDERING ROAD
CONDITIONS**

By

Qingqing Xie

A Thesis

Submitted to the Faculty of Graduate Studies

through the Department of Electrical and Computer Engineering

in Partial Fulfillment of the Requirements for

the Degree of Master of Applied Science at the

University of Windsor

Windsor, Ontario, Canada

© 2018 Qingqing Xie

**MODELING AND SIMULATION OF PM MOTOR TESTING ENVIRONMENT
TOWARDS EV APPLICATION CONSIDERING ROAD CONDITIONS**

By

Qingqing Xie

APPROVED BY:

B. Minaker

Department of Mechanical, Automotive & Materials Engineering

M. Abdelkhalek

Department of Electrical and Computer Engineering

N. C. Kar, Advisor

Department of Electrical and Computer Engineering

06. 18. 2018

AUTHOR'S DECLARATION OF ORIGINALITY

I at this moment certify that I am the sole author of this thesis and that no parts of this thesis have been published or submitted for publication.

I certify that, to the best of my knowledge, my thesis neither infringes upon anyone's copyright nor violates any proprietary rights and that any ideas, techniques, quotations, or any other material from the work of other people included in my thesis, published or otherwise, are fully acknowledged in accordance with the standard referencing practices. Furthermore, to the extent that I have included copyrighted material that surpasses the bounds of fair dealing within the meaning of the Canada Copyright Act, I certify that I have obtained a written permission from the copyright owner(s) to include such material(s) in my thesis and have included copies of such copyright clearances to my appendix.

I declare that this is a true copy of my thesis, including any final revisions, as approved by my thesis committee and the Graduate Studies Office, and that this thesis has not been submitted for a higher degree to any other University or Institution.

ABSTRACT

The electric vehicle (EV) performance testing is an indispensable aspect of the design study and marketing of electric vehicle. The development of a suitable electric motor testing environment for EVs is very significant. On the one hand, it provides a relatively realistic testing environment for the study of the key technologies of electric vehicles, and it also plays an essential role in finding a reasonable and reliable optimization scheme. On the other hand, it provides a reference to the evaluation criteria for the products on the market. This thesis is based on such requirements to model and simulate the PM motor testing environment towards EV applications considering road conditions.

Firstly, the requirements of the electric motor drive as a propulsion system for EV applications are investigated by comparing to that of the traditional engine as a propulsion system. Then, as the studying objective of this work, the mathematical model of PMSM is discussed according to three different coordinate systems, and the control strategy for EV application is developed. In order to test the PM motor in the context of an EV, a specific target vehicle model is needed as the virtual load of the tested motor with the dyno system to emulate the real operating environment of the vehicle.

A slippery road is one of the severe driving conditions for EVs and should be considered during the traction motor testing process. Fuzzy logic based wheel slip control is adopted in this thesis to evaluate the PM motor performance under slippery road conditions. Through the proposed testing environment, the PM motor can be tested in virtual vehicle driving conditions, which is significant for improving the PM motor design and control.

DEDICATION

To My Family and Friends

ACKNOWLEDGEMENT

I wish to express my sincere gratitude to my advisor Dr. Kar for his assistance at every step of the way. His guidance has had an immense influence on my professional growth, and without his technical expertise, reviews, and criticism it would not have been possible to shape this thesis. I would also like to thank my committee members Dr. Minaker and Dr. Abdelkhalek for their valuable suggestions and guidance in the completion of this work.

I would like to show my appreciation for my CHARGE lab mates, who always are patient to help me out whenever I have difficulties, especially during the transitional period of from mechanical engineering to electrical engineering and my thesis writing. I also would like to thank my dear friends, who have always been by my side and encouraged me when I am down. Their love and support are invaluable.

TABLE OF CONTENTS

AUTHOR’S DECLARATION OF ORIGINALITY	III
ABSTRACT	IV
DEDICATION.....	V
ACKNOWLEDGEMENT	VI
LIST OF TABLES	X
LIST OF FIGURES	XI
NOMENCLATURE.....	XIII
1 INTRODUCTION.....	1
1.1 OVERVIEW.....	1
1.2 ELECTRIC MOTOR REQUIREMENTS FOR EV APPLICATIONS	2
1.3 PM MOTOR FOR EV APPLICATIONS.....	6
1.4 BACKGROUND STUDY	10
1.5 CONTRIBUTIONS AND RESEARCH OBJECTIVES	12
1.6 THESIS OUTLINE.....	12
2 PMSM MODELING AND CONTROL STRATEGY	14
2.1 PMSM MATHEMATICAL MODEL	14
2.1.1 <i>PMSM model in A-B-C stationary coordinate system.....</i>	<i>15</i>
2.1.2 <i>PMSM model in α-β coordinate system</i>	<i>18</i>
2.1.3 <i>PMSM model in d-q-o synchronous rotation coordinate system.....</i>	<i>20</i>
2.2 PMSM CONTROL STRATEGY FOR EV APPLICATION.....	22
2.2.1 <i>MTPA control under the motor base speed.....</i>	<i>24</i>
2.2.2 <i>Flux-weakening control strategy above the motor base speed.....</i>	<i>27</i>
2.2.3 <i>The implementation process of vector control strategy.....</i>	<i>30</i>

2.3	PROPOSED PMSM DRIVE SIMULATION MODEL AND THE RESULTS	30
3	VEHICLE MODELING.....	34
3.1	ELECTRIC VEHICLE SIMULATION METHODS	34
3.1.1	<i>Forward simulation</i>	34
3.1.2	<i>Backward simulation</i>	35
3.1.3	<i>Forward /backward simulation</i>	36
3.2	VEHICLE DYNAMICS MODELING	37
3.2.1	<i>Traction force and driving resistance forces</i>	37
3.2.2	<i>Tire ground adhesion and maximum tractive effort</i>	40
3.2.3	<i>Longitudinal equations of motion</i>	42
3.2.4	<i>Tire-road model</i>	44
3.2.5	<i>The model of vehicle dynamics</i>	46
3.3	VEHICLE LOAD MODELING.....	47
3.4	VERIFICATION OF SIMULATION MODEL.....	51
4	FUZZY LOGIC BASED WHEEL SLIP CONTROL.....	52
4.1	INTRODUCTION TO WHEEL SLIP CONTROL.....	52
4.2	CONTROL ALGORITHMS OF WHEEL SLIP	53
4.2.1	<i>Logic threshold control</i>	53
4.2.2	<i>PID control</i>	54
4.2.3	<i>Sliding mode variable structure control</i>	55
4.2.4	<i>Neural network control</i>	57
4.2.5	<i>Fuzzy logic control</i>	57
4.3	FUZZY LOGIC-BASED WHEEL SLIP CONTROL	59
4.3.1	<i>Overview of Fuzzy logic control</i>	59
4.3.2	<i>Development of fuzzy logic controller based on optimal wheel slip ratio</i>	61
4.3.3	<i>Wheel slip ratio calculation</i>	66
4.3.4	<i>PM motor testing environment with fuzzy logic-based wheel slip control</i>	68
4.4	SIMULATION RESULTS AND ANALYSIS	69
4.4.1	<i>UDDS test under the dry concrete road condition</i>	70

4.4.2	<i>HWFET test under the dry concrete road condition</i>	73
4.4.3	<i>UDDS test under the snowy road condition</i>	75
5	CONCLUSIONS AND FUTURE WORK	78
5.1	CONCLUSIONS	78
5.2	FUTURE WORK	79
	REFERENCES	80
	LIST OF PUBLICATIONS	86
	APPENDIX	87
	VITA AUCTORIS	89

LIST OF TABLES

Table 1.1 The comparison between IM, PMSM and SR motor	7
Table 1.2 List of electric vehicles.....	9
Table 2.1 Partial parameters of the chosen IPMSM.....	22
Table 3.1 Coefficient of Rolling Resistance.....	39
Table 3.2 Average values of coefficient of road adhesion	41
Table 3.3 The parameters of Magic Formula under four common road surfaces.....	45
Table 4.1 Fuzzy rule base.....	65

LIST OF FIGURES

Fig. 1.1 Example torque-speed characteristic of a traction machine.	5
Fig. 1.2 Comparison of a torque-speed characteristic of traction motor and engine.	6
Fig. 2.1 PMSM coordinate system.	15
Fig. 2.2 PMSM coordinate system.	23
Fig. 2.3 MTPA current trace	27
Fig. 2.4. Voltage Limitation circle.	29
Fig. 2.5. Motor speed.....	31
Fig. 2.6. Motor torque.	32
Fig. 2.7. Three-phase current.....	32
Fig. 2.8. Schematic of PMSM drive model.	33
Fig. 3.1. Structure of forward simulation.	35
Fig. 3.2. Structure of backward simulation.	35
Fig. 3.3. Structure of forward/backward simulation.	36
Fig. 3.4. The total forces acting on a two-axle vehicle.....	43
Fig. 3.5. μ - λ curve of the four different roads.	45
Fig. 3.6. Schematic diagram of the vehicle dynamics model.	46
Fig. 3.7. Schematic of vehicle load.	49
Fig. 3.8. Schematic of verification of vehicle load model.	50
Fig. 3.9. Verification results of vehicle load model.	50
Fig. 3.10. The required driving torque based on UDDS.....	50
Fig. 3.11. The required torque comparison between ADVISOR and the Simulink model.....	51
Fig. 4.1. PID control diagram.....	54
Fig. 4.2. The diagram of sliding mode variable structure control.....	56
Fig. 4.3. Principle block diagram of fuzzy logic control.	58
Fig. 4.4. The basic components of the fuzzy control system.	61

Fig. 4.5. The block diagram of fuzzy logic based wheel slip control.	62
Fig. 4.6. Fuzzy membership functions: (a) input error; (b) error change rate; (c) adjust torque.	64
Fig. 4.7. 3D representation of fuzzy rule base.	66
Fig. 4.8 Stress analysis of the driving wheel	67
Fig. 4.9. The PI controller-based driver model.....	69
Fig. 4.10. The overall structure of PM motor testing environment simulation.....	69
Fig. 4.11. Required motor operation points for UDDS.	71
Fig. 4.12. UDDS reference speed vs wheel speed.....	72
Fig. 4.13. Simulated vehicle speed and wheel speed for UDDS.	72
Fig. 4.14. The power of the PM motor under UDDS.	72
Fig. 4.15. Required motor operation points for HWFET	73
Fig. 4.16. HWFET reference speed vs wheel speed.	74
Fig. 4.17. Simulated vehicle speed and wheel speed for HWFET.	74
Fig. 4.18. The power of the PM motor under HWFET.	74
Fig. 4.19. Vehicle speed and reference speed without slip control.....	76
Fig. 4.20. Wheel slip ratio without slip control.	76
Fig. 4.21. Adjusted motor torque and reference motor torque.	77
Fig. 4.22. Vehicle speed with slip control.	77

NOMENCLATURE

Generally, symbols have been defined locally. The list of principle symbols is given below

$u_A, u_B, u_C,$: A, B, C three-phase stator windings voltage respectively
$i_A, i_B, i_C,$: A, B, C three-phase stator windings current respectively
L_A, L_B, L_C	: self-inductance of the stator windings respectively
u_α, u_β	: stator voltage of α -axis and β -axis respectively
i_α, i_β	: stator current of α -axis and β -axis respectively
$L_\alpha, L_\beta,$: self-inductance of the stator in α -axis and β -axis respectively
$M_{\alpha\beta}, M_{\beta\alpha}$: mutual inductance of the stator in α -axis and β -axis respectively
u_d, u_q	: stator voltage of d-axis and q-axis respectively
i_d, i_q	: stator current of d-axis and q-axis respectively
$L_d, L_q,$: self-inductance of the stator in α -axis and β -axis respectively
R_s	: Stator windings resistance
ψ_r	: flux produced by the rotor
p	: number of pole pairs
J	: inertia of the motor
B	: friction coefficient of the motor
T_m	: mechanical load torque
T_e	: electromagnetic torque
T_L	: load of the motor
$\omega_m(\omega), \omega_e$: mechanical and electrical rotor rotating speed respectively
G	: Transmission gear ratio
η	: Mechanical efficiency of driveline
m	: mass of the vehicle
g	: acceleration of gravity
α	: slope angle of the road
f_r	: rolling resistance coefficient

F_t	: traction force
F_f	: rolling resistance force
F_g	: grade force
F_d	: aerodynamic drag force
F_a	: acceleration resistance force
ρ	: air density
C_d	: aerodynamic drag coefficient of the vehicle
A_f	: cross-sectional area of the vehicle
δ	: mass factor
F_x	: longitudinal friction force
F_z	: vertical force
u	: friction coefficient
λ	: slip ratio
$T_w (T_t)$: torque applied to the wheels
T_m	: torque produced by the motor
h_g	: height of center of gravity
I_m, I_t, I_w	: inertia of motor, transmission, wheel separately
L_a	: length from center of gravity to front axle
L_b	: length from center of gravity to rear axle
L	: wheelbase
F_{xf}	: longitudinal tire force at the front tires.
F_{xr}	: longitudinal tire force at the rear tires
F_{aero}	: equivalent longitudinal aerodynamic drag force
R_{xf}	: force due to rolling resistance at the front tires
R_{xr}	: force due to rolling resistance at the rear tires

1 INTRODUCTION

1.1 Overview

The concept of the electric vehicle (EV) has existed since the first EV was made in the mid-nineteenth century. The internal combustion engine (ICE) vehicle was more competitive and more appealing to automakers and customers due to the low cost of oil during that time. Over the last decades, however, EV has emerged as one of the most active and fruitful areas for research in the automobile industry and academia, especially the topics related to batteries and electric motors, which are the critical technologies for EV development. That is due to the increasing awareness of environmental pollution and a shortage of the fossil fuels alongside the benefits of EVs, such as low energy consumption, high energy efficiency, high energy recuperation and more available energy source as well as low environmental pollution. Because EVs are still in their commissioning and developing stage, they have not widely been accepted by the majority of consumers. There are a few solutions to address the bottlenecks of promoting EVs in the market, such as the development of a high-performance battery pack, improvement of the efficiency of the driving system, and construction of fast charging stations [1]. Among the above, it is of great significance to develop an electric motor drive system with high performance and low energy consumption.

The determination of accurate electric motor drive system performance is essential for the development of advanced EV powertrains in order to extend the driving distance range of EVs. Electric motors and drives need to be more efficient, lighter and more compact. At the EV design and preliminary validation stages, various electric vehicle simulation and testing methods are utilized to evaluate the performance of the electric motor to determine its efficiency and maximum operating performance over a wide speed range. Test results assist in optimal component sizing and weight reduction of the vehicle powertrain. This thesis focuses on the development of a testing environment where the electric motor can be tested in the context of an EV. It provides a

comparatively accurate representation of real on-road test data for electric motor design and optimization.

Depending on the application of electric motors, they have to meet some specific requirements in terms of performance, efficiency, and safety. To achieve an accurate representation of real on-road test data, road conditions, such as road surface and road gradient, should be considered. They also need to be realistic to meet the EV real-time performance constraints. It is especially true when the phenomenon of wheel slip occurring on a slippery road will directly affect the traction/braking control strategy developing, which is associated with the output of the traction motor. A high wheel slip rate occurs during the vehicle operation when the increase of the wheel speed is much greater than that of the vehicle. This may happen if the driver keeps pushing the acceleration pedal to force more torque to reach the desired speed. Without wheel slip ratio restriction, there exist potential safety issues when the required torque exceeds the capability. For example, permanent magnet synchronous motors (PMSM) will produce constant speed unconcerned of the motor load only if the load is within the capability of the motor. If the external torque load is more than the torque produced by the motor, it will slip out of synchronism and will come to rest. It is necessary to consider road conditions in studying electric-drive performance in vehicle level and develop a targeted traction motor testing environment for EV application.

1.2 Electric motor requirements for EV applications

Electric motors are pervasive in our everyday lives, found in pretty much all that we use from automobiles to kitchen appliances to IOT-connected and smart devices. Thus, it is more important than ever to understand the machine characteristics, control techniques, and associated interactions with electronic drives that power the machines depending on the application of electric motors, so that they can meet the specific requirements in terms of performance, efficiency, and safety. For the study of traction motors, it is significant to investigate the requirements of an electric motor for EV

application to improve the design and control of traction motors and develop an appropriate testing platform.

After more than one hundred years of reform and development, the automobile has become more than a simple means of transport. The automobile in the 21st century needs to be optimized in combination with engineering and practical applications in terms of factors that include power, handling, comfort, safety, aesthetics, energy saving, emission reduction, life expectancy, and so on. Similar to the internal combustion engine driving system, the electric motor drive system of the electric vehicle also has the goal of improving the dynamic performance, economy and comfort. The traction motors for EV applications belong to the category of medium and low voltage motors. Due to their specific application, they have higher performance requirements than general low-voltage products. The primary requirements are as follows [2], [3], [4]:

- Convenient for layout: with high power density and compact design of the electric motor, its controller can save a lot of space and reduce the weight of the vehicle as well in some degree.
- Extended driving range: by reducing the controller switching losses, motor copper loss and iron loss, the efficiency is improved, so that the electric motor drive system can extend the driving range under certain conditions of battery capacity.
- Wide speed range: the vehicle has two types of working conditions, one of which requires the work to be in the constant torque region when starting, accelerating, and climbing. In the other type, at high speed, the motor is required to work in the constant power region.
- High maximum vehicle speed: increase speed limit of the motor in constant torque realm to achieve the maximum vehicle speed.
- Steep ramp start: high torque output at low motor speed, and fast response at starting.
- Regenerative braking ability: the electric motor acts as a generator to convert the braking energy into electrical energy to charge the battery, especially in the

frequent starting and stopping of city driving, which can efficiently improve the driving range.

- Conformity to driving habits: by raising the torque control accuracy, the smooth and linear control of the throttle torque can be obtained, so that the driving experience of the electric vehicle is close to or even better than that of the traditional vehicle.
- Low operation noise: with the advantage of high-frequency switching state, the noise from the motor and controller is reduced, thus reducing the noise pollution on the environment and improving the ride comfort.
- High tolerance in severe operation conditions: It is able to guarantee reliability and safety and ensures long service time in which the vehicle is experiencing situations such as bumpy road surfaces and complicated weather such as high winds, dust, high humidity, etc.
- Cater to the market demand: it is necessary to optimize the design to ensure a reasonable production cost and the convenience of repairing and follow-up maintenance.

From the torque-speed characteristic of electric machine perspectives, Fig. 1.1 shows a typical load profile with a limited battery voltage that is expected to be fulfilled by a traction motor [5]. Operation of an electric machine is described by its torque-speed characteristics curve, a curve that shows the change in torque as a function of rotation speed. Regarding the motor speed range, it can be identified by two characteristic realms.

A first region corresponds to operation at constant torque and therefore to an increase of power with speed. Within this range, the counter-electromotive force increases in direct proportion to the speed. Consequently, the supply voltage delivered to the motor by the inverter reaches its limit with the battery voltage. The corresponding speed is a crucial characteristic of the motor as well as its power supply, and it is known as the base speed (S_{base}). In a transient condition, the maximum torque can only be maintained for a very short period due to the thermal limit of the motor or the physical limit of the power electronics.

Above the base speed, it is expected to produce constant power. At the point when the motor speed reaches the base speed, the inverter additionally achieves its maximum voltage, and the current is likewise at the most extreme. Subsequently, the inverter cannot supply any further power to the motor, and hence it is called “ constant power region,” also referred to as “flux weakening zone”. The reason is that if there is a need to increase the speed of the vehicle above base speed, at that point the yield torque of the motor must be diminished. Subsequently, the flux is debilitated to accomplish the decrease in the torque.

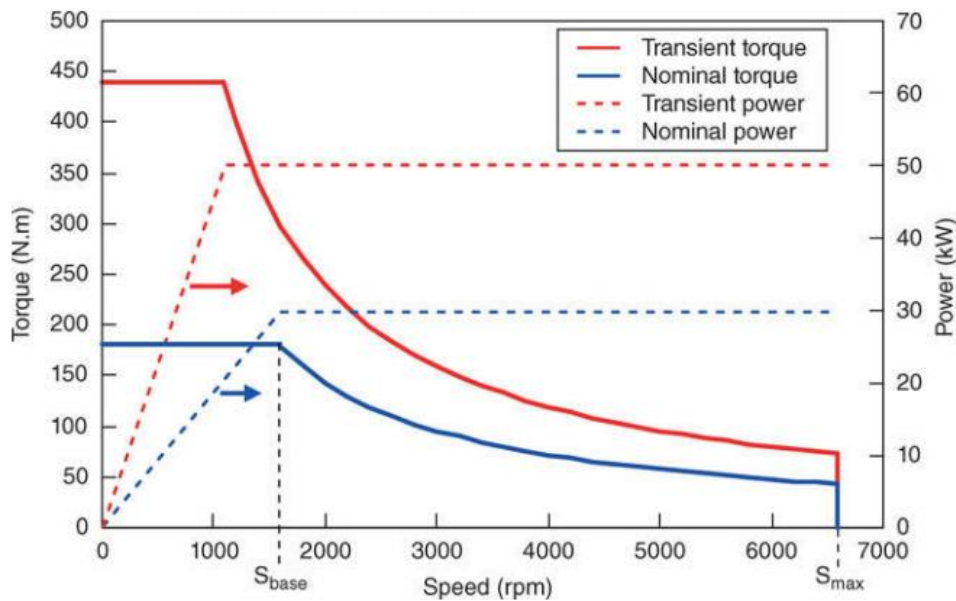


Fig. 1.1 Example torque-speed characteristic of a traction machine.

In terms of characteristics of the motor and engine, the challenge of the electric vehicle is somehow different from that of a traditional engine vehicle. The output torque of an engine increases with the increase of engine speed before the peak speed of the engine; then the torque decreases with engine speed up after the speed peak point, especially for a gasoline engine, shown as Fig. 1.2 [6]. In order to achieve more traction force on driving wheels at the low-speed region, a transmission is required for the vehicle.

The engine would operate consistently in the high-efficiency realm by adjusting the transmission ratio of the gearbox. The ideal characteristic of the electric motor can be implemented through improving the design of the motor control strategy to obtain high torque at low speed, constant power at high speed, which can conduct direct drive by eliminating the transmission, and eventually, reduce the cost and improve the total efficiency. With the development of electronic technology and optimizing the control strategy, the electric motors are able to operate in a wide speed range to achieve a high efficiency of energy conversion.

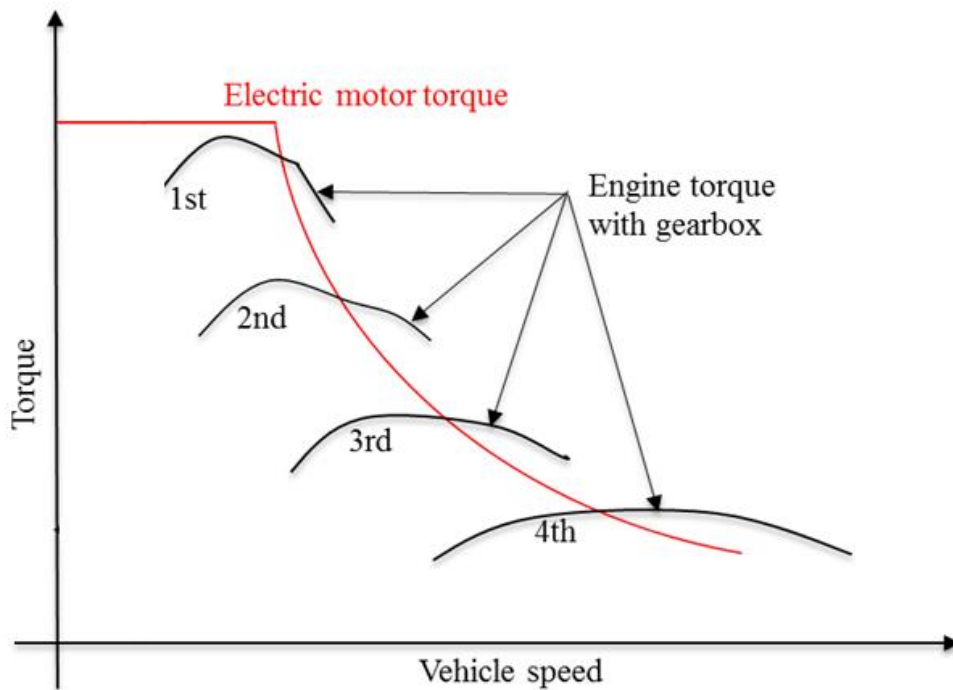


Fig. 1.2 Comparison of a torque-speed characteristic of traction motor and engine.

1.3 PM motor for EV applications

From the above discussion, it is clear what to expect from the electric motor and what to aim for when designing the electric motor for EV application. There are three main types of electric motors utilized currently for traction applications: induction motor

(IM), permanent magnet synchronous motor (PMSM), and switched reluctance motor (SRM). Each of them has its merits and demerits relying on the operating conditions and the requirements. Regarding the characteristics and performance of the electric motor, Table 1.1 shows a summary of the comparison between induction, PM and SR motors [7], [8], [9].

Table 1.1 The comparison between IM, PMSM and SR motor

Parameter	PM motor	Induction motor	SR motor
Power density	High	Average	High
Efficiency (%)	95-97	94-95	<90
High speed range	4000-10000	9000-15000	<15000
Weight	Low	Average	Low
Reliability	Average	High	Average
Overload capacity	Average	High	High
Service life	High	High	High
Structural robustness	Average	High	Average
Vibration	Low	Low	High
Noise	Low	Low	High
Control	Hard	Simple	Simple
Technology maturity	Low	High	Average

Induction motor: Induction motors are considered the most reliable and cost-effective motors volume wise. They are the most widely-used motors in all industries. As we know, to produce torque an electric machine needs two interacting fluxes. For the fluxes, one originates from the stator called stator flux, and the other is from the rotor called rotor flux. According to Faraday's and Lenz's laws, the rotor flux of the induction motor is generated due to the rotating flux from the stator and afterward both the fluxes interact with each other and deliver torque. Similar to the DC motor, there is no need for an outside arrangement to power its rotor in an induction motor, which makes manufacturing and operation simpler. With this particular structural advantage, the control of an induction motor is relatively simple to implement, very robust, and does not

require high maintenance. The mechanical stability of the aluminum rotor bars, however, must be considered at very high speeds. Induction motors have been available since long ago, and the manufacturing process has been enhanced which makes them competitive in terms of cost.

Switched reluctance motor: An SRM is a kind of motor doubly salient with phase coils mounted around diametrically opposite stator poles. There are no slip rings, windings or permanent magnets on the rotor of an SRM. The rotor is a piece of steel, and the shape of the rotor creates salient poles, and the stator has concentrated coils. SRMs have a robust and straightforward structure. Thus they are suitable for the applications that require low speed, high torque, and wide speed range. However, due to higher control requirements, serious pulsating torque, noise and large size, SRMs have not been widely adopted in the application of commercial electric vehicles.

Permanent magnet synchronous motor: PMSMs can be seen as a DC motor where the rotor is replaced with permanent magnets. The stator coils produce rotating flux when supplied with a three-phase AC source. The flux generated by the magnets in the rotor interacts with the stator flux and produces torque. The rotor flux in PM motors, however, cannot be controlled and has impacts on the design of the motor. In general, over IM and SRM, the PM motor has many advantages that make it the most competitive traction motor for EV applications, including high torque and power density, high efficiency, compactness, low weight and high torque at low speed.

As Table 1.2 shows the current dominant popular existing EVs in the market (all the information from the product specifications), there is a high percentage of automakers that chose PM motor as a propulsion mechanism. According to present technology states of the electric motor development and the requirements of EV applications, the advantages of a PM motor make it the best candidate for EVs among the various options [8].

Table 1.2 List of electric vehicles

Brand of BEV	Motor type	Motor power	Motor Torque
Tesla model S 85D	Induction motor	310 kW	600 Nm
Chevrolet Spark EV	PM motor	105 kW	327 Nm
Chevrolet Bolt EV	PM motor	150 kW	360 Nm
Ford Focus Electric	PM motor	106 kW	250 Nm
Fiat 500e	PM motor	83 kW	200 Nm
Kia Soul EV	PM motor	81.4 kW	285 Nm
Renault Zoe Expressior	Synchronous motor	65/88 kW	220/250Nm
Mitsubishi i-MiEV	PM motor	49 kW	197 Nm
Toyota RAV4 EV	Induction motor	115kW	296 Nm
Honda Fit EV	PM motor	92 kW	256 Nm
Nissan Leaf SL	Synchronous motor	80 kW	280 Nm
Volkswagen e-Golf	Synchronous motor	85 kW	270 Nm
Mercedes B-class EV	Induction Motor	132 kW	340 Nm
Smart Fortwo EV	PM motor	55 kW	130 Nm
BMW i3	PM motor	125 kW	250 Nm

Through the overview of the dominant traction motors in the market, PM motors have been the most promising candidates for EV applications at present. Improving the performance of PM motors is becoming a hot topic by improving the design and control strategy. Consequently, a comprehensive and accurate testing method to estimate whether the electric motor meets the requirements of an EV's propulsion system is essential since it directly reflects the overall performance of the EV.

1.4 Background Study

In general, electric motor testing contains routine tests which follow industry test standards, such as IEEE standards, SAE standards, and specific performance tests which depend on the requirement for applications. Routine tests for industrial electric motors include measurement of power, current input at no-load and rated voltage, and current input with a locked rotor at rated voltage. Those tests need to acquire necessary data for determining efficiency, power factor, starting torque, pull-up torque, breakdown torque, and rated-load temperature rise [10]. These parameters do not show much about the specific performance of EVs. For instance, an efficiency test of industrial motors involves simple power measurements at a few different loads. These working conditions are quite unlike the dynamic changes that traction motors and drivetrains encounter. The specific performance test is expected to give a thought of how traction motors are likely to perform in real life application.

Industrial electric motors are rated with considerably higher efficiencies than the motors used in EVs as the efficiency of these motors is measured only while the motor powers its rated load. The efficiency rating does not consider other operational factors, such as the amount of time the motor spends accelerating to a certain speed or coasting to a stop. For many industrial motor applications, acceleration time and coasting time are negligible. Therefore, these factors might not be necessary. In the case of EVs, however, the motor spends a considerable part of its operational time either accelerating or decelerating. When characterizing the traction motor, its performance during these periods cannot be ignored. So, one can see that traction motors for EVs and hybrid electric drivetrains operate in dynamic environments that are very different from industrial motors.

For the study of the performance of electric motors as propulsion systems in electric vehicles, there are three primary methods currently used for this study, which are software-based system simulation, hardware-in-the-loop (HIL) simulation with a test platform, and on-road vehicle testing [11]. The software-based method is less costly, more practical and flexible. It, however, lacks realism and real-time performance. Despite

the drawbacks of this method, it has significant meaning in the early stages for estimating machine parameters and performance to speed up a designer's understanding of when different control and machine design assumptions are applicable [12], [13], [14]. The on-road test method is based on the traditional vehicle testing approach, including traffic road driving test and test site testing, which involves the actual use of the road or a particular test site to test the car in the operation of the movement and performance. It has good fidelity, while it is costly, rigid and difficult to test and analyze the results [11]. It is usually adopted before mass production. HIL with the tester method is designed through the combination of software and hardware approaches. Since it combines some of the advantages of the previous two methods, this method is quite popular for studying the components and rapid prototyping of electric motors and drives [15], [16], [17]. The software-based method is the primary option to verify the reasonability of proposal methods because of the advantage of low cost, time efficiency and flexibility. In this work, a software-based method is adopted to model and simulate a PM motor testing environment towards EV applications.

Researchers and engineers have done much work in the study of electric-drive propulsion. Most of them used a motor test bench associated with a dynamic vehicle model to emulate an electric vehicle for different study objectives, such as traction motor design [18] and control [19], [20], [21], and the behavior of the electric motor in vehicle level [22], [23]. In this case, it is necessary to have a vehicle dynamic model with the capability of simulating the actual EV under various environmental conditions to guarantee the accuracy and fidelity of the results. The factors that affect the accuracy of the vehicle dynamics model includes road surface, road gradient, weather conditions, wheel slip phenomenon and rotational inertia. In the literature, several papers consider the road gradient and wind speed as constant or zero in their vehicle dynamics models [11], [16], [18], [23]. Moreover, some often neglect the effect of the different weather conditions in term of wheel slip and road friction coefficient [18], [23], [24], such as rain and snow. The rotational inertia of each component is ignored in some cases [25]. Therefore, it is valuable to develop a vehicle dynamics model that considers the above factors to provide more realistic EV operation conditions for the study of electric-drive.

1.5 Contributions and research objectives

The objective of this thesis is to model and simulate a PM motor testing environment towards EV applications considering road conditions, which can implement the PM motor test in the context of an EV. Compared to the existing test methods, the proposed method with an advanced vehicle model can provide more realistic EV operating conditions during the test in order to achieve more accurate results. The PM motor can be tested under different drive cycles, such as UDDS or HWFET. By integrating fuzzy logic based wheel slip ratio control into the load motor, the reaction of PM motor can be emulated as the vehicle is driving on the slippery road.

This study contributes to provide more precise required torque results for PM motor control and achieve better fidelity of overall test results by developing an advanced vehicle dynamic model considering road conditions and wheel slip. Also, the proposed testing environment allows the PM motor to be tested as the vehicle is running under different road conditions, especially, a slippery road. Analysis of PM motor speed-torque performance under different drive cycles and road conditions can improve the PM motor design and control development for EV applications. To implement the method, the following items are need to be conducted: 1) model a PMSM with vector control; 2), Develop a vehicle dynamics model considering the road conditions and wheel slip; 3) develop fuzzy logic-based wheel slip ratio control; and 4) integrate the wheel slip feedback control into the dyno motor.

1.6 Thesis Outline

This thesis is organized as follows:

Chapter 2: This chapter focuses on three dominant primary methods of modeling a PMSM, and the control strategy adopts MTPA and flux-weakening.

Chapter 3: For this chapter, simulation methods of an electric vehicle are discussed, and the suitable method for this study is selected. Vehicle dynamics model and vehicle load model are developed by considering the different road

conditions (e.g., road surface), which the tire-road model can simulate different road surfaces.

Chapter 4: In this chapter, the key area of interest is in developing wheel slip control. The investigation of wheel slip control algorithm is conducted and a fuzzy logic based wheel slip control is selected for this study. A fuzzy logic-based wheel slip controller is developed based an optimal wheel slip ratio. With the predefined road conditions, the simulation of the vehicle employing the PM motor is conducted for UDDS & HWFET and the result is analyzed.

2 PMSM MODELING AND CONTROL STRATEGY

The PMSM drive is the PM motor with the corresponding controller. The control strategy needs to be based on the mathematical model of PMSM. In this chapter, based on the establishment of the appropriate simplified mathematical model of PMSM, the control strategy is developed and suitable for EV application.

2.1 PMSM mathematical model

The study of electric machine system needs to be based on a mathematical model. The inserted PMSM used in this work has a stator with an A, B, C three-phase symmetric winding, inserted permanent magnets on the rotor, and non-damped windings on the rotor surface, which means that the air gap magnetic field between the stator and the rotor is disturbed. Because of the relative motion between the stator and the rotor, the relationship between parameters is complex and time-varying. It is challenging to conduct quantitative analysis and mathematical modeling directly. To simplify the model, the following assumptions need to be made:

- 1) The back emf is sinusoidal;
- 2) The inductance versus rotor position is sinusoidal;
- 3) The eddy current and hysteresis losses in the motor are not calculated;
- 4) The current in the motor is a strong wave current of symmetry B
- 5) The saturation and parameter changes of the motor are neglected;

Based on these assumptions, the analysis of the complicated electromagnetic relationship inside the motor can be implemented, and the error of the obtained results and the actual situation is within the allowable range of engineering projects [26].

2.1.1 PMSM model in A-B-C stationary coordinate system

The differential equations of PMSM are classified into three forms of expression: three-phase stationary coordinate system (A-B-C), two-phase stationary coordinate system (α - β) and two-phase synchronous rotating coordinate system (d-q-0). In the stationary three-phase coordinate system, the axis of the stator A-phase winding is taken as the reference axis of the space coordinate system, and the established A-B-C coordinate is shown in figure 2.1. A-axis, B-axis and C-axis are spatially corresponding to the A, B, C axis of the three-phase stator windings respectively; θ represents the angle of rotation of the direct axis (d-axis) of the rotor through the A-phase winding; ψ_r is the excitation flux linkage generated by the rotor; i_s is the integrated vector of the three-phase current of the stator. ω is the motor speed. The two-phase stationary coordinate system (α - β) and two-phase rotating synchronous coordinate system (d-q-0) will be introduced below.

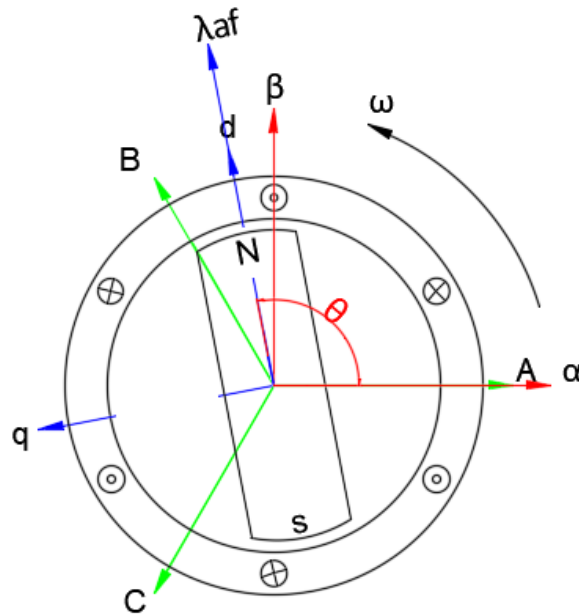


Fig. 2.1 PMSM coordinate system.

Considering the physical quantities involved in PMSM include electricity, magnetism, torque, and rotor speed, its mathematical model needs to be composed of stator voltage equations, stator flux linkage equations, electromagnetic torque equations and motion equations. In the A-B-C stationary three-phase coordinate system, taking the Y-connection stator winding as an example, the stator voltage is the neutral voltage, which is the sum of the voltage drop caused by the current passing through the stator resistance and the induced electromotive force of the stator flux linkage changing over time.

The stator voltage equation is:

$$\begin{bmatrix} u_A \\ u_B \\ u_C \end{bmatrix} = \begin{bmatrix} u_N \\ u_N \\ u_N \end{bmatrix} + \begin{bmatrix} R_s & 0 & 0 \\ 0 & R_s & 0 \\ 0 & 0 & R_s \end{bmatrix} \begin{bmatrix} i_A \\ i_B \\ i_C \end{bmatrix} + \frac{d}{dt} \begin{bmatrix} \Psi_A \\ \Psi_B \\ \Psi_C \end{bmatrix} \quad (2.1)$$

Where u_A, u_B, u_C and i_A, i_B, i_C correspond to the A, B, C three-phase stator windings voltage and current respectively; R_s is the resistance of stator windings; u_N is the neutral potential of the windings; and Ψ_A, Ψ_B, Ψ_C are the three-phase stator flux linkage respectively. The equation (2.1) can be rewritten as:

$$u_s = u_N + R_s i_s + \frac{d\Psi_s}{dt} \quad (2.2)$$

The three-phase stator flux linkage is the sum of the stator winding armature reaction flux and the flux between the permanent magnets of the rotor and each winding of the stator. The stator flux linkage equation is:

$$\begin{bmatrix} \Psi_A \\ \Psi_B \\ \Psi_C \end{bmatrix} = \begin{bmatrix} L_A & M_{AB} & M_{AC} \\ M_{BA} & L_B & M_{BC} \\ M_{CA} & M_{CB} & L_C \end{bmatrix} \begin{bmatrix} i_A \\ i_B \\ i_C \end{bmatrix} + \Psi_r \begin{bmatrix} \cos \theta \\ \cos(\theta - \frac{2}{3}\pi) \\ \cos(\theta + \frac{2}{3}\pi) \end{bmatrix} \quad (2.3)$$

Where L_A, L_B, L_C are the self-inductances of the stator windings respectively; $M_{XY} = M_{YX}$ ($X=A, B, C; Y=A, B, C; X \neq Y$) is the mutual inductance of the stator windings; Ψ_r is the flux produced by the rotor; and θ is the lead angle of the rotor direct-axis rotating through the stator A-phase.

The electromagnetic torque can be expressed as:

$$T_e = p\Psi_r \left[i_A \sin \theta + i_B \sin(\theta - \frac{2}{3}\pi) + i_C \sin(\theta + \frac{2}{3}\pi) \right] \quad (2.4)$$

The mathematical model of PMSM in the A-B-C stationary three-phase coordinate system cannot be simply analyzed by symmetry in terms of its electrical and magnetic structures, as there is relative motion between the stator and rotor in space. Meanwhile, this model of the stator flux linkage equations contains a variable θ , which is the angle of the rotor direct-axis rotating through the A-phase winding. So, the stator flux linkage equations are a set of nonlinear time-varying equations related to the rotor's instantaneous position. The electromagnetic torque equation of the motor is based on the stator flux linkage, introducing the above variable θ , which is also a nonlinear time-varying equation. Therefore, the mathematical model established in the coordinate system is cumbersome, adding to the design difficulty of the system controller in analysis and application. In the A-B-C stationary three-phase coordinate system, it is difficult to analyze the electromagnetic relationship of PMSM and control strategy. Hence it is necessary to find a more convenient mathematical model.

2.1.2 PMSM model in α - β coordinate system

In an α - β stationary two-phase coordinate system, the variables of the PMSM can be directly measured, so it is feasible to establish the mathematical model in this system. As shown in Fig. 2.1, the axis of the stator A-phase windings is taken as the α -axis of the α - β coordinate system and the axis of leading α -axis by the angle of $\frac{\pi}{2}$ is taken as the β axis. The current variables can be represented by the coordinate transformation in the A-B-C stationary three-phase coordinate system. The coordinate transformation from an A-B-C stationary three-phase coordinate system to an α - β stationary two-phase coordinate system is the Clarke Transform, with the transformation matrix:

$$C_{ABC/\alpha\beta} = \frac{2}{3} \begin{bmatrix} 1 & -\frac{1}{2} & -\frac{1}{2} \\ 0 & \frac{\sqrt{3}}{2} & -\frac{\sqrt{3}}{2} \end{bmatrix} \quad (2.5)$$

The transformation matrix from the α - β stationary two-phase coordinate system to A-B-C stationary three-phase coordinate system is:

$$C_{\alpha\beta/ABC} = \begin{bmatrix} 1 & 0 \\ -\frac{1}{2} & \frac{\sqrt{3}}{2} \\ -\frac{1}{2} & -\frac{\sqrt{3}}{2} \end{bmatrix} \quad (2.6)$$

Therefore, the stator current of α -axis i_α and β -axis i_β can be represented in the form of the stator current i_A , i_B and i_C in the A-B-C coordinate system, represented as:

$$\begin{bmatrix} i_\alpha \\ i_\beta \end{bmatrix} = \frac{2}{3} \begin{bmatrix} 1 & -\frac{1}{2} & -\frac{1}{2} \\ 0 & \frac{\sqrt{3}}{2} & -\frac{\sqrt{3}}{2} \end{bmatrix} \begin{bmatrix} i_A \\ i_B \\ i_C \end{bmatrix} \quad (2.7)$$

The stator voltage of α -axis, u_α and β -axis, u_β can be represented as:

$$\begin{bmatrix} u_\alpha \\ u_\beta \end{bmatrix} = R_s \begin{bmatrix} i_\alpha \\ i_\beta \end{bmatrix} + \frac{d}{dt} \begin{bmatrix} \Psi_\alpha \\ \Psi_\beta \end{bmatrix} \quad (2.8)$$

In the α - β coordinate system, the stator flux linkage equation can be expressed as:

$$\begin{bmatrix} \Psi_\alpha \\ \Psi_\beta \end{bmatrix} = \begin{bmatrix} L_\alpha & M_{\alpha\beta} \\ M_{\beta\alpha} & L_\beta \end{bmatrix} \begin{bmatrix} i_\alpha \\ i_\beta \end{bmatrix} + \Psi_r \begin{bmatrix} \cos \theta \\ \sin \theta \end{bmatrix} \quad (2.9)$$

Where L_α , L_β are the self-inductance of the stator in the α -axis and the β -axis respectively; and $M_{\alpha\beta}$, $M_{\beta\alpha}$ are the mutual inductance of the stator in the α -axis and the β -axis respectively. Moreover, those can also be derived as:

$$\begin{aligned} \begin{bmatrix} L_\alpha & M_{\alpha\beta} \\ M_{\beta\alpha} & L_\beta \end{bmatrix} &= \begin{bmatrix} \frac{L_d + L_q}{2} + \frac{L_d - L_q}{2} \cos 2\theta & \frac{L_d - L_q}{2} \sin 2\theta \\ \frac{L_d - L_q}{2} \sin 2\theta & \frac{L_d + L_q}{2} - \frac{L_d - L_q}{2} \cos 2\theta \end{bmatrix} \\ &= \begin{bmatrix} L_d \cos^2 \theta + L_q \sin^2 \theta & (L_d - L_q) \sin \theta \cos \theta \\ (L_d - L_q) \sin \theta \cos \theta & L_d \sin^2 \theta + L_q \cos^2 \theta \end{bmatrix} \end{aligned} \quad (2.10)$$

The electromagnetic torque in the α - β coordinate system can be expressed as:

$$T_e = p(\Psi_\alpha i_\beta - \Psi_\beta i_\alpha) \quad (2.11)$$

After the coordinate transformation, the mathematical model of PMSM has been simplified in the α - β stationary two-phase coordinate system. For the salient pole of PMSM, there is $L_d \neq L_q$ due to the existence of the salient pole effect. For the non-salient pole of PMSM, there is $L_d = L_q$ in the ideal case, and the mathematical model can be further simplified. However, the stator flux linkage equation and voltage equation are still

non-linear time-varying equations that contain the variable θ . This mathematical model of PMSM in α - β coordinate system still needs to be further simplified.

2.1.3 PMSM model in d-q-o synchronous rotation coordinate system

To simplify the nonlinear time-varying equations, the variable θ should be avoided. For this purpose, the coordinate system is bound from the stationary edge of the angle θ to the rotating edge of the angle θ to establish a new rotating coordinate system. As shown in Fig. 2.1, the direct axis (d-axis) is the direction of rotor excitation flux linkage (magnetic pole center axis), and the quadrature axis (q-axis) leads the d-axis by an angle of $\frac{\pi}{2}$ in the d-q-0 coordinate system. The current variables can be represented by the coordinate transformation using the values in the A-B-C stationary three-phase coordinates system.

Through a Park Transformation, the transformation matrix from an α - β stationary two-phase coordinate system to a d-q-0 synchronous rotating coordinate system is:

$$C_{\alpha\beta/dq} = \begin{bmatrix} \cos\theta & \sin\theta \\ -\sin\theta & \cos\theta \end{bmatrix} \quad (2.12)$$

The transformation matrix from the d-q-0 synchronous rotating coordinate system to the α - β stationary two-phase coordinate system is:

$$C_{dq/\alpha\beta} = \begin{bmatrix} \cos\theta & -\sin\theta \\ \sin\theta & \cos\theta \end{bmatrix} \quad (2.13)$$

After substituting equation (2.13) into equation (2.7) to obtain the stator current in d-axis i_d , and q-axis i_q , they can be represented in the form of the stator current i_A , i_B and i_C in the A-B-C coordinate system, which is expressed as:

$$\begin{bmatrix} i_d \\ i_q \end{bmatrix} = \sqrt{\frac{2}{3}} \begin{bmatrix} \cos \theta & \cos(\theta - \frac{2\pi}{3}) & \cos(\theta + \frac{2\pi}{3}) \\ -\sin \theta & \sin(\theta - \frac{2\pi}{3}) & -\sin(\theta + \frac{2\pi}{3}) \end{bmatrix} \begin{bmatrix} i_A \\ i_B \\ i_C \end{bmatrix} \quad (2.14)$$

The stator voltage of d-axis, u_d and q-axis, u_q can be represented as:

$$\begin{bmatrix} u_d \\ u_q \end{bmatrix} = R_s \begin{bmatrix} i_d \\ i_q \end{bmatrix} + \frac{d}{dt} \begin{bmatrix} \Psi_d \\ \Psi_q \end{bmatrix} - \omega \begin{bmatrix} \Psi_q \\ \Psi_d \end{bmatrix} \quad (2.15)$$

In the d-q-0 coordinate system, the stator flux linkage equation can be expressed as:

$$\begin{bmatrix} \Psi_d \\ \Psi_q \end{bmatrix} = \begin{bmatrix} L_d & 0 \\ 0 & L_q \end{bmatrix} \begin{bmatrix} i_d \\ i_q \end{bmatrix} + \Psi_r \begin{bmatrix} 1 \\ 0 \end{bmatrix} \quad (2.16)$$

The electromagnetic torque in the d-q-0 coordinate system can be expressed as:

$$T_e = \frac{3}{2} p [\Psi_r i_q + (L_d - L_q) i_d i_q] \quad (2.17)$$

According to the moment balance, the motor motion equation in the d-q-0 coordinate system is:

$$T_e - T_L - B\omega = J \frac{d\omega}{dt} \quad (2.18)$$

Here, ω is the motor mechanical angular speed; J is the inertia of the motor; B is the friction coefficient; T_L is the load of the motor. This equation is also suitable for the A-B-C coordinate system and the α - β coordinate system. From equation (2.15) to equation (2.18), it can be seen that the mathematical model of PMSM in the d-q-0 coordinate system obtained by coordinate transformation successfully avoids the variable θ , and the stator voltage equation and stator flux linkage equation are constant coefficient equations, which facilitate further calculations and analysis.

According to equation (2.17), the electromagnetic torque of a PMSM is produced jointly by the permanent magnet rotor excitation flux and salient pole effect. For the torque control of inserted PMSM ($L_d \neq L_q$), it is necessary to control the d-axis current and the q-axis current at the same time, while for the surface mounted PMSM ($L_d = L_q$), the d-axis current is 0 and only the q-axis current is required to be controlled. Therefore, according to the d-q-0 synchronous rotating coordinate system, the mathematical model of a PMSM can be used to implement closed-loop torque control in vector control easily.

2.2 PMSM control strategy for EV application

In this thesis, IPMSM is selected as the object of study and the parameters of the motor are shown in Table 2.1. The control methods of a PMSM mainly include vector control and direct torque control. Here, the vector control method is adopted. According to the characteristics of different vector control methods, the appropriate vector control strategy is selected and implemented in the MATLAB/SIMULINK environment. The details will be discussed further below.

Table 2.1 Partial parameters of the chosen IPMSM

Items	Parameters
Rated voltage	275 V
Rated current	64 A
Rated power	24 kW
Rated speed	3880 rpm
Rated torque	60 Nm
Peak torque	160 Nm
Q-axis inductance	0.376 mH
D-axis inductance	0.232 mH
Magnet flux linkage	0.15
Number of pole pairs	4
Motor inertia	0.089 kgm ²

The control strategy of a PMSM for the electric vehicle is MTPA control below base speed and flux weakening control above base speed [27]. The purpose of MTPA control is to maximize torque per unit current, which can make full use of the potential of the motor to maximize energy use. The significance of flux weakening control is that when the motor angular speed is higher than the base speed, which is restricted by the power supply voltage; the back electromotive force brought by the motor rotation is close to the supply voltage and the angular speed cannot be increased. Meanwhile, the d-axis of the motor needs to be reversed current, resulting in a demagnetization effect, so partially offsetting the flux generated by the permanent magnet can raise the motor speed.

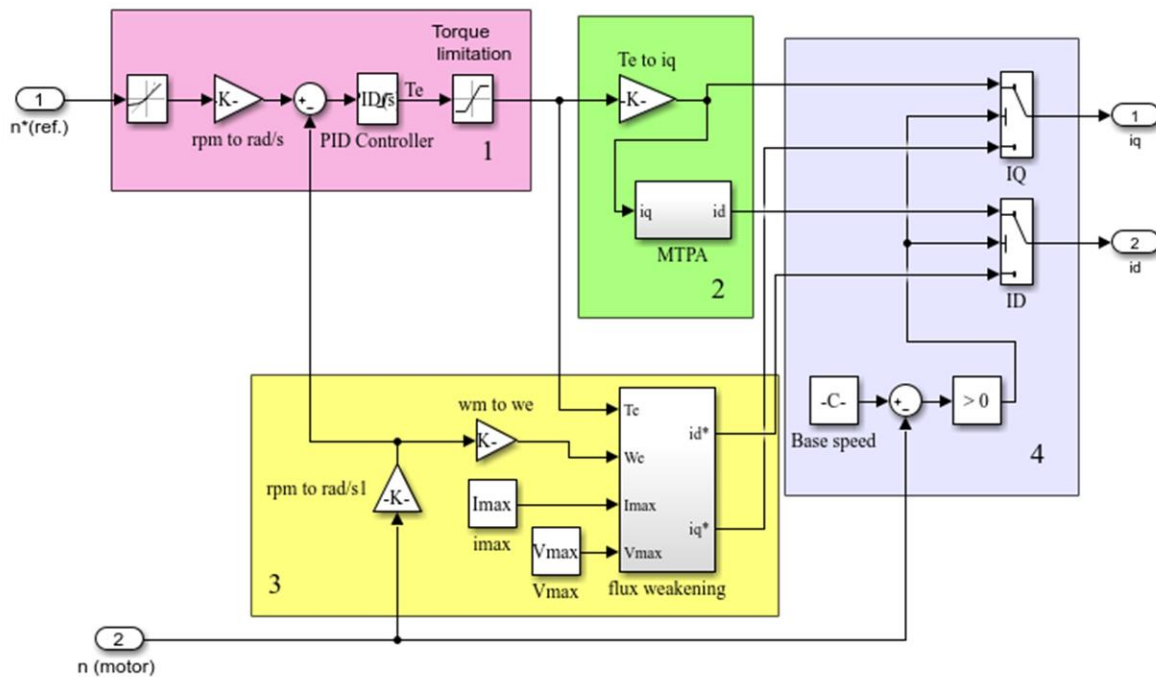


Fig. 2.2 PMSM coordinate system.

The control strategy module of the electric motor based on vector control is shown in Fig. 2.2. The inputs of the current control strategy module are the desired speed, current speed, and the outputs are the quantities of i_d and i_q . It mainly includes the torque limitation module (area 1), the control strategy switching module (area 4), the MTPA control (area 2) and the flux weakening control (area 3). The function of the torque

limitation module is to limit the output of the desired torque according to the out power and speed of the motor. The role of the control strategy switching module is to determine if the current speed reaches the base speed to switch the flux weakening control. Otherwise, the MTPA control is maintained. The two modules are respectively the implementation of MTPA strategy and flux weakening strategy. The following two sections will describe the details of MTPA and flux weakening strategies.

2.2.1 MTPA control under the motor base speed

The traction motor of electric vehicle needs frequent acceleration and deceleration, especially under urban conditions. Therefore, from the perspective of energy saving and extending the driving range, it is necessary to achieve the required electromagnetic torque with minimum current through a control strategy.

The current motor speed determines the switching point between the two strategies. Therefore, the current control strategy in vector control is based on the motor speed to determine the control strategy. The control strategy is developed based on the peak power of the selected motor. The implementation of MTPA strategy is discussed below.

According to the mathematical model of PMSM based on the d-q-0 coordinate system, it is easy to get:

$$I_s = \sqrt{i_d^2 + i_q^2} \quad (2.19)$$

If γ is the angle between i_d and i_q axes, there is:

$$\begin{cases} i_d = -I_s \sin \gamma \\ i_q = I_s \cos \gamma \end{cases} \quad (2.20)$$

According to equation (2.20), the electromagnetic torque equation is:

$$T_e = \frac{3}{2} p [\psi_r I_s \cos \gamma - \frac{1}{2} (L_d - L_q) I_s^2 \sin 2\gamma] \quad (2.21)$$

The goal of MTPA is to generate the maximum output torque per ampere current, which is equal to the maximum value of equation (2.21). The Extreme Value Theorem is

used to find the first derivative of equation (2.21). When the first derivative is 0, the result is:

$$\psi_r I_s \sin \gamma - (L_d - L_q) I_s^2 \cos 2\gamma = 0 \quad (2.22)$$

Substituting $\cos 2\gamma = 2 \cos^2 \gamma - 1$ into equation (2.22) obtains:

$$\cos \gamma = \frac{\sqrt{\psi_r^2 + 8(L_d - L_q)^2 I_s^2} - \psi_r}{4(L_d - L_q) I_s} \quad (2.23)$$

According to equation (2.23), the relationship between i_d and i_q can be obtained:

$$i_d = \frac{\sqrt{\psi_r^2 + 4(L_d - L_q)^2 i_q^2} - \psi_r}{2(L_d - L_q)} \quad (2.24)$$

Substituting equation (2.24) into equation (2.17), the relationship between T_e and i_q under MTPA control strategy can be obtained:

$$T_e = \frac{1}{2} p i_q \left[\sqrt{\psi_r^2 + 4(L_d - L_q)^2 i_q^2} + \psi_r \right] \quad (2.25)$$

From equation (2.25), it can be seen that in practical applications, the magnetic permeability of permanent magnetic material and air is different in most cases. There are $L_d \neq L_q$ and $\cos \gamma \neq 0$, so $i_d = I_s \cos \gamma \neq 0$. Only for ideal non-salient pole PMSMs ($L_d = L_q$), there is $\cos \gamma = 0$, so $i_d = I_s \cos \gamma = 0$. The maximum electromagnetic torque per unit current control strategy is degraded to $i_d = 0$ control.

In the case of non-uniform air gap permeance, there are two possible relationships between the direct-axis inductance and the quadrature-axis inductance. From equation (2.24), when $L_d < L_q$, there is $i_d < 0$. At this moment, $\frac{\pi}{2} < \gamma < \frac{3\pi}{2}$, the armature reflects the demagnetizing effect. The maximum electromagnetic torque per unit current control strategy aims to increase the power factor by weakening the excitation magnetic field, thereby increasing the electromagnetic torque. When $L_d > L_q$, there is $i_d > 0$. At this

moment, $-\frac{\pi}{2} < \gamma < \frac{\pi}{2}$, the armature reflects the magnetizing effect, the control strategy aims to increase the power factor by enhancing the rotor excitation magnetic field, thus increasing the electromagnetic torque.

The limitation of this control strategy is that there is a motor base speed (ω_b). When the current motor speed is greater than ω_b , the current, i_d, i_q cannot be controlled by the same control strategy because of the limitation of voltage. This situation will be discussed in the next section (2.2.2).

The implementation of this method is to calculate the value of i_q based on the target electromagnetic torque, T_e^* from equation (2.25), then to calculate the value of i_d from equation (2.24). After limiting processing, the target three-phase currents can be obtained through equation (2.14) then sent to the inverter.

Considering $i_d < 0$, the operating curve of the system under the MTPA control is shown in Fig. 2.3, where the value of the curve in the figure is calculated based on the selected IPMSM parameter in this study. The blue trajectory is the current limitation circle, representing the maximum operating current permitted by the motor (175 A).

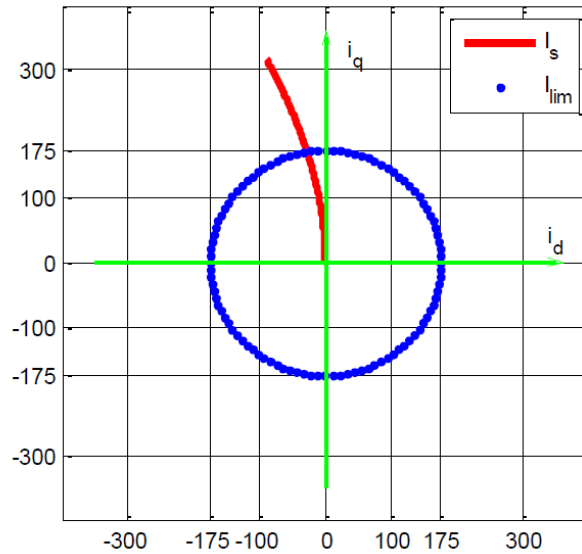


Fig. 2.3 MTPA current trace

2.2.2 Flux-weakening control strategy above the motor base speed

IPMSM flux weakening control is designed to improve the motor speed above the base speed, which can effectively extend the motor speed range. This section focuses mainly on implementing the flux weakening control strategy.

The vector control is implemented using SVPWM, and the maximum line voltage output during SVPWM modulation is $U_{DC}/\sqrt{3}$. The induction electromotive force can be expressed as:

$$E_s = \omega_e \sqrt{(L_q i_q)^2 + (\psi_f + L_d i_d)^2} \quad (2.26)$$

Under the conditions above, the relation between the maximum speed and current can be obtained. When the back EMF reaches the limit, U_{lim} , the following equation holds:

$$\left(\frac{U_{lim}}{\omega} \right)^2 = (L_q i_q)^2 + (\psi_f + L_d i_d)^2 \quad (2.27)$$

When $L_d \neq L_q$, equation (2.27) becomes an elliptical function. Different motor speeds ω form a number of curves, and the curves are called voltage limit circles. The elliptic curvature decreases with the increase of ω , and the center of the ellipse is at $(-\frac{\psi_f}{L_d}, 0)$.

In order to set the expected value as the input of the motor and apply the flux weakening control strategy, another input of the rotor, the electrical angular speed, ω_e , is required. Rewriting the expected current as:

$$\begin{cases} \left(\frac{U_{\lim}}{\omega_e}\right)^2 = (L_q i_q^*)^2 + (\psi_f + L_d i_d^*)^2 \\ T_e^* = \frac{3}{2} p [\psi_r i_q^* - (L_q - L_d) i_d^* i_q^*] \end{cases} \quad (2.28)$$

In equation (2.28), ω_e and T_e^* are the inputs and only i_d^* and i_q^* are unknown. The solution to the equation can be uniquely determined by taking into account the limitations of the current limit circle and the current sign, namely:

$$\begin{cases} i_d^* = f(T_e^*, \omega_e) \\ i_q^* = f(T_e^*, \omega_e) \end{cases} \quad (2.29)$$

The equation (2.29) can be rearranged as follows:

$$\begin{cases} i_d^* = \frac{1}{L_d} \left(-\psi_f + \sqrt{\left(\frac{U_{\lim}}{\omega_e}\right)^2 - L_q i_q^*} \right) \\ T_e^* = \frac{3}{2} p \left[\psi_f i_q^* - (L_q - L_d) \frac{i_q^*}{L_d} \left(-\psi_f + \sqrt{\left(\frac{U_{\lim}}{\omega_e}\right)^2 - (L_q i_q^*)^2} \right) \right] \end{cases} \quad (2.30)$$

Here, i_d^* and i_q^* are calculated respectively from the given T_e^* and ω_e . Equation (2.27) is used to determine the scope of the flux weakening control. The rated voltage of 275 V is the RMS value of line voltage; and the DC bus voltage is the peak line voltage $U_{DC} = 275\sqrt{2} = 388.85V$. According to the principle of flux weakening control, i_d is reversely increased to offset part of ψ_r , and the current within the current limit circle is used for demagnetization in order to obtain the maximum ω_e . From the equation (2.27), U_{lim} will take 224V to get:

$$\omega_{e-\max} = \frac{U_{\lim}}{\psi_f + L_d i_d} \quad (2.31)$$

The base speed is the corresponding motor speed at the intersection of the current path and the current limit circle during the MTPA control. From the motor parameter information, it can be determined that the peak current is 175 A and the base speed ω_b is 358.161 rad/s from the equations (2.20), (2.23), (2.27).

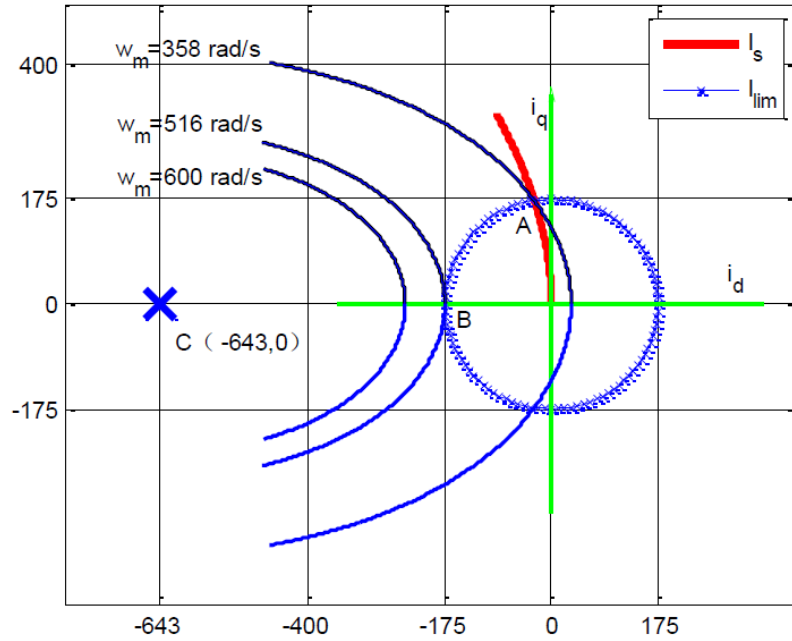


Fig. 2.4. Voltage Limitation circle.

Fig. 2.4 is a composite diagram of the voltage limitation circle and the previous MTPA current trace calculated from equation (2.27) based on the parameters of IPMSM. Point A is the intersection of the voltage limit circle, the current limit circle, and the MTPA trace, which corresponds to the base speed. Point B is the maximum speed that can be reached under flux weakening control when the IPMSM theoretically outputs 0 torque (the values in the figure are approximate). Point C is the center of all voltage limit circles, $(-\frac{\Psi_f}{L_d}, 0)$, which is within the current limit circle and indicates that the motor

does not have the maximum power output capacity [28]. Consequently, the range of

output torque is $[0, 160]$ (Nm) as the motor is operating in flux-weakening realm within speed of $[358, 516]$ (rad/s).

2.2.3 The implementation process of vector control strategy

MTPA strategy calculation process

- 1) Determine the power curve, input the desired torque and measurement speed;
- 2) Determine the DC bus current range $I_s \in [0, I_{lim}]$ according to the motor parameters;
- 3) Calculate the current phase in the MTPA range from the scope of I_s by a certain step length based on equation (2.23);
- 4) Calculate i_q^* through equation (2.25) based on the target electromagnetic torque;
- 5) Calculate i_d^* through equation (2.24);

Flux weakening strategy calculation process

- 1) Determine the base speed from the equations (2.20), (2.23), and (2.27);
- 2) Determine the scope of the limit voltage and torque;
- 3) Determine the range of current and voltage for loop calculations, based on equation (2.23) to obtain i_d^* and i_q^* .

The above calculation process should consider the step length of calculation. The improper selection of step length will lead to the unsmooth curve after interpolation, and the output curve of the motor will be worse.

2.3 Proposed PMSM drive simulation model and the results

The overall schematic of the proposed PMSM drive mode is shown in Fig. 2.8. In order to verify the correctness of the built simulation, the simulation conditions are set as

follows: the reference speed is set to $N_{ref} = 1000$ r/min, the torque at the initial moment is set to $T_L = 3N \cdot m$; and at $t = 0.05s$, the load torque is set to $T_L = 1N \cdot m$. The simulation results are shown in Fig. 2.5. In addition, the variation of other variables can be observed according to the actual needs. Here only the change of three variables are listed: the motor speed, electromagnetic torque, and three-phase current. The simulation results show that when the motor speed rose from zero to the reference speed of 1,000 rpm, although the motor speed is somehow overshooting at the beginning due to the PI speed controller, it then has a fast-dynamic response speed. As the motor load suddenly decreases at $t = 0.05s$, the motor can also quickly return to a given reference speed, thus verifying the correctness of the simulation model and illustrating that the control strategy can meet the operational requirement.

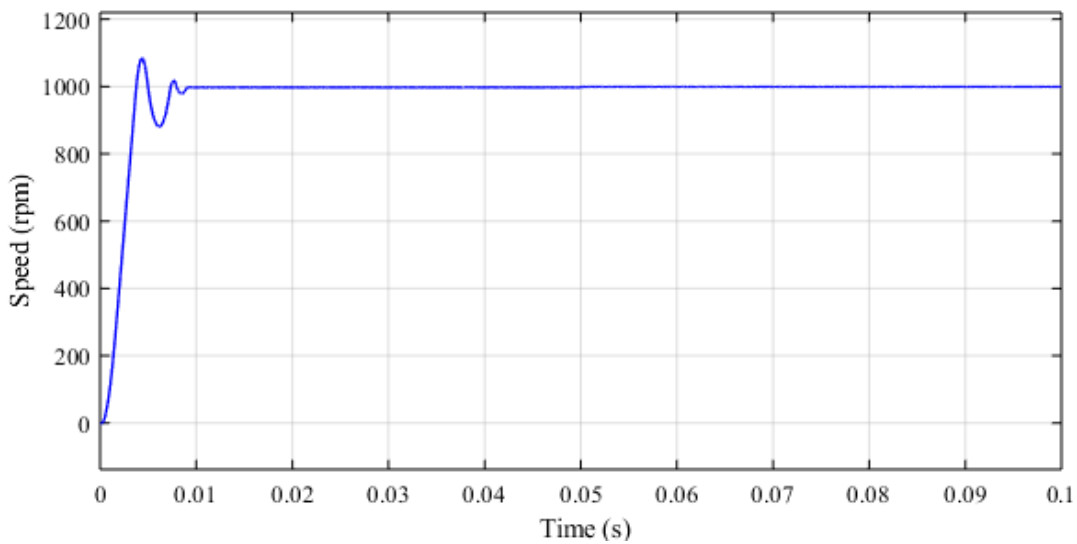


Fig. 2.5. Motor speed.

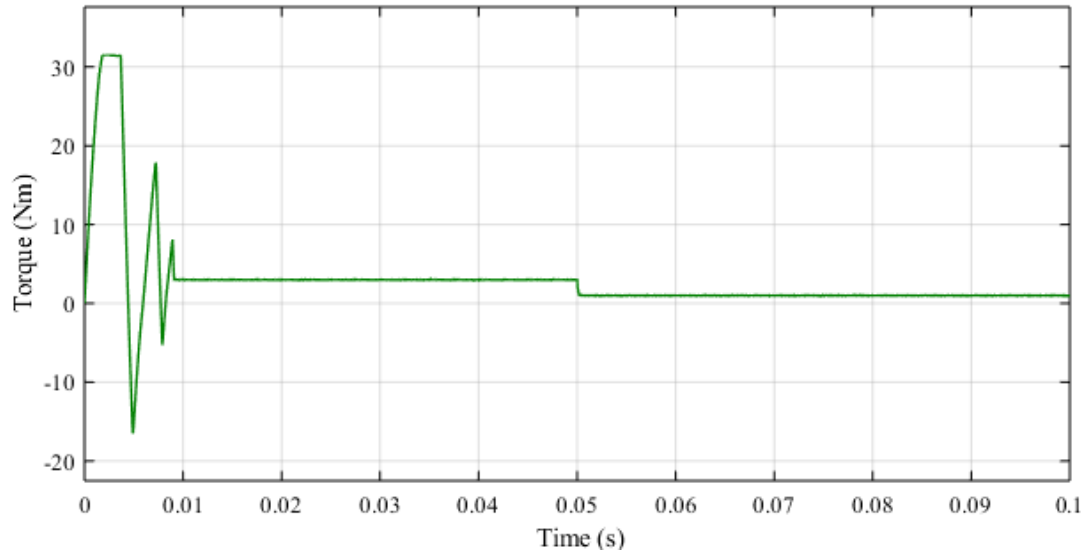


Fig. 2.6. Motor torque.

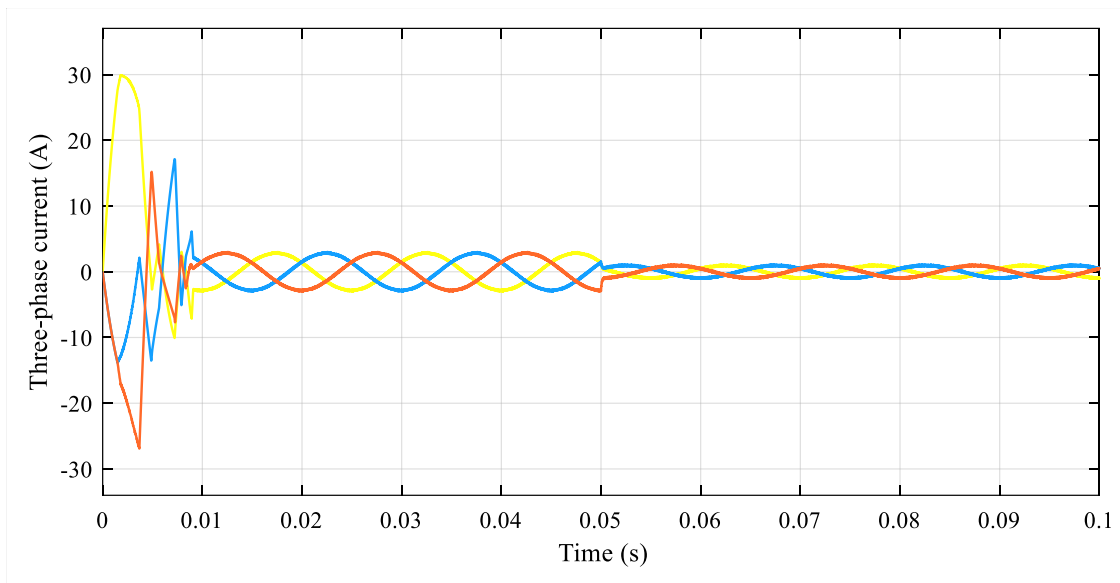


Fig. 2.7. Three-phase current.

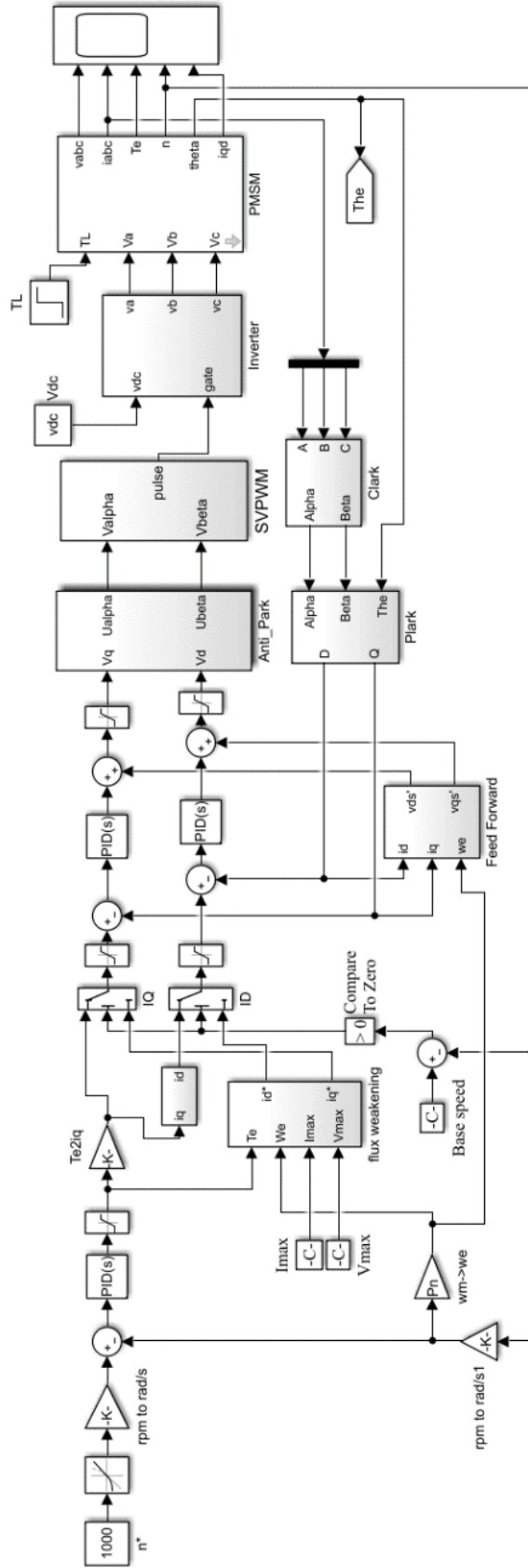


Fig. 2.8. Schematic of PMSM drive model.

3 VEHICLE MODELING

To test the electric motor in context of an EV with a tester, the vehicle dynamics model is required and associated with a dyno motor to emulate the performance of the electric motor used in an EV. Depending on the study objective and the complexity of the vehicle model, the methods of electric vehicle simulation are discussed, and a suitable simulation method and reasonable vehicle dynamics model is selected.

3.1 Electric vehicle simulation methods

The methods of electric vehicle simulation can generally be divided into two types according to the direction of power flow: forward simulation and backward simulation. The combined forward/backward approach is also adopted in some vehicle modeling tools such as ADVISOR.

3.1.1 Forward simulation

The biggest difference between forward simulation and backward simulation is the presence or absence of a driver model. There is a driver model present in the forward simulation. Its role is to create appropriate acceleration and brake commands in real time according to the required speed and the present speed, and it commonly adopts a proportional-integral-derivative (PID) controller. The controller can conduct energy management according to the driver's intention. The commands from the driver model are usually converted into torque delivered by the motor. Then the torque is the input of the transmission model, which can convert the torque according to the efficiency and gear ratio of the transmission. In turn, the torque from the transmission is delivered forward to the drivetrain, toward the actual physical power flow in the vehicle, until the point when it brings about a tractive force at tire/road interface. The structure of forward simulation is shown in Fig. 3.1.

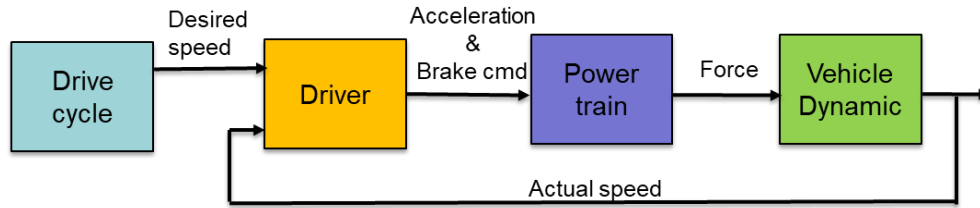


Fig. 3.1. Structure of forward simulation.

The forward approach is especially advantageous as it represents the behavior of a real vehicle and driver. Since forward models are addressed in quantities measurable in a physical drivetrain, the vehicle controller can be developed and tested in simulations. Likewise, vehicle dynamics models can be incorporated in a forward vehicle model. Also, this method is adaptable for calculating the maximum effort acceleration, as they are completely open throttle occasions. This approach is adopted by vehicle modeling tools like AMESim, PSAT [29].

3.1.2 Backward simulation

By contrast, the backward simulation model does not consider the driver's intention, so there is no driver model presented [30]. This simulation model starts from the requirements of the system, first assuming that the vehicle can be driven according to the predefined drive cycles, and then determining how each drivetrain component should perform to meet the requirements of the drive cycle. In this architecture, the required driving torque for driving the vehicle is calculated in real time at each time step in accordance with the required vehicle speed trace and transmitted in the opposite direction of the actual torque transmission route. The structure of the backward simulation is shown in Fig. 3.2.

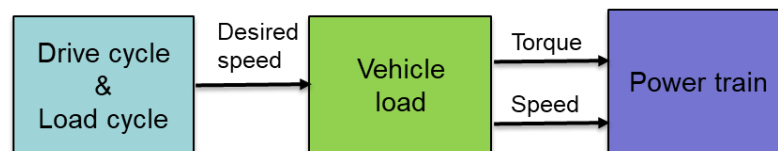


Fig. 3.2. Structure of backward simulation.

The backward-facing approach is convenient because automotive drivetrain components tend to be tested so that a table of efficiency or loss versus output torque and speed is developed. This approach implies that a straightforward calculation can determine a component's efficiency and allow the calculation to progress [31], [32].

3.1.3 Forward /backward simulation

Some vehicle modeling tools adopt the combined backward/forward approach, such as ADVISOR. ADVISOR's approach is unique in the way it handles the component performance limits in its backward-facing stream of calculations and in the addition of a simple forward stream of predictions. Depending on the demand for this study, the combined forward/backward simulation method is adopted. The structure of the proposed simulation is shown in Fig. 3.3. The forward simulation focuses on the behavior of a real vehicle, which the test motor drive acts as the propulsion system. The backward simulation aims to provide the load condition for the test motor as the driving condition of the actual vehicle.

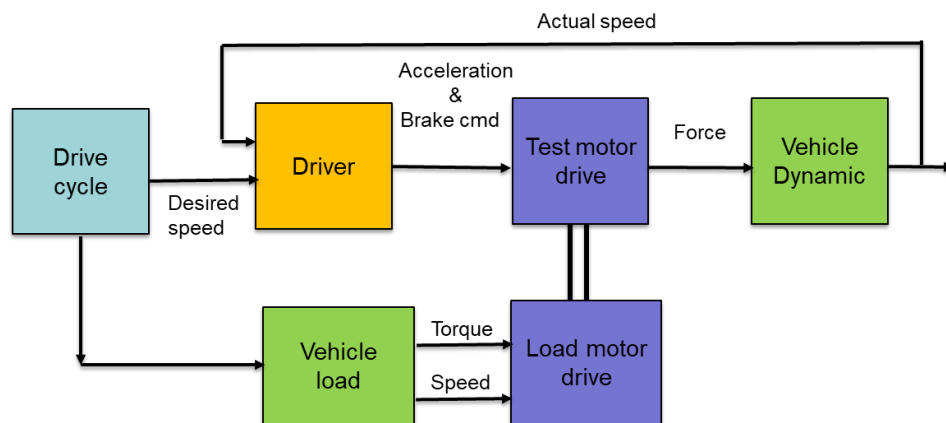


Fig. 3.3. Structure of forward/backward simulation.

3.2 Vehicle dynamics modeling

For the type of vehicle dynamics studied in this thesis, where the power flow between the motor and wheels will be analyzed, it is reasonable to assume that the vehicle has a rigid body, which can be modeled as a lumped mass at the vehicle's center of gravity [33]. Moreover, only longitudinal vehicle dynamics is considered, and straight-line motion is simulated, which is of interest while under the assumption that vehicle stability is not violated under any conditions. Vehicle dynamics expect to describe how a vehicle moves on a road surface while it is affected by forces between the tire and the road, as well as aerodynamics and gravity. The understanding of vehicle dynamics is equally important while evaluating the powertrain's effect on the vehicle's performance (usually assessed through simulations).

3.2.1 Traction force and driving resistance forces

Traction force: In an electric vehicle, the torque generated by the traction motor is transmitted to the driving wheel via the transmission system. At this moment, the torque acting on the driving wheel produces circumferential force F_0 on the ground, facing the reaction force F_t of the drive-wheel, which is the external force that drives the vehicle, namely, traction force. The expression is

$$F_t = \frac{T_t}{r} \quad (3.1)$$

where T_t is the torque acting on the driving wheel, and r is the radius of the wheel.

The torque T_t is from the traction motor through the transmission system to the driving wheel. Assuming T_m is the traction motor torque; G represents the transmission ratio; η represents the mechanical efficiency of driveline, there are

$$T_t = T_m G \eta \quad (3.2)$$

$$F_t = \frac{T_m G \eta}{r} \quad (3.3)$$

Rolling resistance force: Rolling resistance is caused by some different phenomena taking place in and around the car tires during rolling. One of the major effects is that the repeated deflection of the tire causes a hysteresis within the tire material, which gives rise to an internal force resisting the motion [34]. The rolling resistance force, F_f acting on a vehicle in the longitudinal direction, is usually expressed as the effective normal load of the vehicle multiplied by the dimensionless rolling resistance coefficient, f_r as

$$F_f = f_r mg \cos(\alpha) \quad (3.4)$$

where m is the vehicle mass, g is the gravity constant, α is the road angle.

There are several factors affected the rolling resistance force of a vehicle. They include the structure and operating conditions of the tire, driving speed, road surface, etc. For example, as a passenger vehicle drives on concrete road, the relationship between rolling coefficient f_r , and driving speed (up to 128 km/h) can be presented as [34]

$$f_r = 0.01(1 + \frac{v}{100}) \quad (3.5)$$

Based on the experimental results, the average values of f_r for different types of the tire under various road surfaces are summarized in Table 3.1

Grade force: When the vehicle goes up, or down a hill, the mass of the vehicle will result in a component which is either opposite of or the same as the direction of motion of the vehicle. This is termed as the grade force F_g . In the case of a road grade, the vehicle's dynamics will be affected by F_g which is parallel with the road as

$$F_g = mg \sin(\alpha) \quad (3.6)$$

where α is the angle between the level road and the horizontal plane. Road slope is often expressed in terms of % grade or degree; here degree will be used throughout the thesis.

Table 3.1 Coefficient of Rolling Resistance

Road surface	Coefficient of rolling resistance f
Pneumatic car tires on	
Large set pavement	0.013
Small set pavement	0.013
Concrete, asphalt	0.011
Rolled gravel	0.02
Tarmacadam	0.025
Unpaved road	0.05
Field	0.1-0.35
Pneumatic truck tires on	
Concrete asphalt	0.006-0.01
Strake wheels in field	0.14-0.24
Track-type tractor in field	0.07-0.12
Wheel on rail	0.001-0.002

Source: *Automotive Handbook*, 7th edition, Bosch, 2007.

Aerodynamic drag force: The aerodynamic drag force is the result of the wind affecting the vehicle during driving, which is unavoidable for any vehicle for which there is air flowing around and/or through the vehicle. The shape of the vehicle and direction of the wind (headwind or tailwind) will impact the aerodynamic drag force F_d . It is partly empirical, and partly based on the expression of dynamical pressure, which is showing a strong dependence on the square of the vehicle speed as

$$F_d = \frac{1}{2} \rho A_f C_d (v + v_{wind})^2 \quad (3.7)$$

where ρ is the air density, C_d the aerodynamic drag coefficient, A_f is the cross-sectional area of the vehicle, v is the vehicle speed and v_{wind} is the component of wind speed moving against the direction of the vehicle.

Acceleration resistance force: When the vehicle speeds up, it needs to overcome the inertia force of its mass to accelerate, which is the acceleration resistance force F_a . The weight of a vehicle is divided into two parts: translational mass and rotating mass. When accelerating, not only does the translational mass produces an inertia force, but also the rotating mass produces an inertia force. To facilitate calculations, the inertia of the rotating mass is generally converted into inertial forces of translational mass. For the car with a fixed gear ratio, mass factor δ is taken as the conversion coefficient of vehicle rotating mass so that the acceleration resistance force can be written as

$$F_a = \delta m \frac{dv}{dt} \quad (3.8)$$

where δ is the mass factor, $\delta > 1$. It mainly relates to the inertia of the powertrain I_p , the inertia of the wheels I_w and the gear ratio of transmission G [35], which is

$$\delta = 1 + \frac{1}{m} \frac{I_w}{r^2} + \frac{1}{m} \frac{G^2 I_p}{r^2} \quad (3.9)$$

3.2.2 Tire ground adhesion and maximum tractive effort

From the above analysis, it can be seen that the traction force provided by the powertrain of the vehicle is an important factor in the vehicle's dynamic performance. In general, the greater the traction force, the better the acceleration performance of the vehicle and the stronger the climbing ability. However, the actual traction force of the vehicle is not only related to the output torque of the powertrain and the effective wheel radius but also closely associated with the adhesion condition of the road. When the road conditions are good, i.e. the tire-road friction coefficient is big enough, a traction force on the driving wheels can be calculated by equation (3.1). When the tire-road friction coefficient is not big enough (e.g., ice and snow road), the wheels tend to slip. At this point, the tangential reaction force to the wheels on the ground is not large, and the traction of the vehicle cannot be reflected. The dynamic performance of the vehicle is not only related to the driving torque of the powertrain, but also restricted by the adhesion conditions of the wheels and the ground.

The coefficient of friction (road adhesion), μ , as in equation (3.10) is the ratio between the longitudinal friction force, F_x , and the vertical force (normal load W), F_z . In Table 3.2 [36], the average values of coefficient of road adhesion for various types of road surfaces are presented.

$$F_x = \mu F_z \quad (3.10)$$

The slip ratio, λ , is different for the case when the vehicle is braking or accelerating, as given by the following relationship:

$$\left\{ \begin{array}{l} \lambda = \frac{r\omega - v}{v} (\text{accelerating}) \\ \lambda = \frac{v - r\omega}{r\omega} (\text{braking}) \end{array} \right. \quad (3.11)$$

where r is the wheel radius, v is the transitional velocity of wheel and equivalent to the velocity of the vehicle (m/s), and ω is rotational velocity of the wheel (rad/s).

Table 3.2 Average values of coefficient of road adhesion

Road surface	Peak value μ_p	Sliding value μ_s
Asphalt and concrete (dry)	0.8-0.9	0.75
Asphalt (wet)	0.5-0.7	0.45-0.6
Concrete (wet)	0.8	0.7
Gravel	0.6	0.55
Earth road (dry)	0.68	0.65
Earth road (wet)	0.55	0.4-0.5
Snow (hard-packed)	0.2	0.15
Ice	0.1	0.07

3.2.3 Longitudinal equations of motion

In the longitudinal direction the major external forces applying on a two-axle vehicle, include the rolling resistance of front and rear tires F_{rf} and F_{rr} , which are represented by rolling resistance moments T_{rf} and T_{rr} , aerodynamic drag force F_d , grading resistance force F_g , and traction force of the front and rear tires, F_{tf} and F_{tr} . F_{tf} is zero for rear-wheel drive vehicle. Otherwise, F_{tr} is zero for a front-wheel drive vehicle. Fig. 3.4 illustrates the total forces acting on a two-axle vehicle. The dynamic equation of motion along the longitudinal direction is presented by [35]

$$M \frac{dv}{dt} = (F_{tf} + F_{tr}) - (F_{rf} + F_{rr} + F_d + F_g) \quad (3.12)$$

where M is the total mass consisted of the vehicle mass, the driver and the rotational equivalent mass.

By summing the moments of all the forces about point R (center of the tire-ground area), the normal load on the front axle W_f can be expressed as

$$W_f = \frac{mgL_b \cos \alpha - T_{rf} + T_{rr} + F_d h_w + mgh_g \sin \alpha + Mh_g dv / dt}{L} \quad (3.13)$$

Similarly, the normal load applying on the rear axle can be determined as

$$W_r = \frac{mgL_a \cos \alpha - (T_{rf} + T_{rr} + F_d h_w + mgh_g \sin \alpha + Mh_g dv / dt)}{L} \quad (3.14)$$

For passenger vehicles, the height of the center of aerodynamic resistance h_w is assumed to be near the height of the center of gravity of the vehicle h_g . The load is determined by the wheelbase L , the distance from the front and rear axles to the center of gravity, L_a , and L_b respectively, and the tire radius r . The equations (3.13) and (3.14) can be rewritten as

$$W_f = \frac{L_b}{L} mg \cos \alpha - \frac{h_g}{L} (F_t - F_r (1 - \frac{r}{h_g})) \quad (3.15)$$

$$W_r = \frac{L_a}{L} mg \cos \alpha + \frac{h_g}{L} (F_t - F_r (1 - \frac{r}{h_g})) \quad (3.16)$$

The tractive effort is restricted by the wheel friction coefficient in the tire to ground contact patch. According to equation (3.10), the maximum tractive effort on the front and rear tires F_{tfmax} and F_{trmax} are expressed as follows:

$$F_{tfmax} = \mu W_f = \frac{\mu mg \cos \alpha (L_b + f_r (h_g - r)) / L}{1 + \mu h_g / L} \quad (3.17)$$

$$F_{trmax} = \mu W_r = \frac{\mu mg \cos \alpha (L_a + f_r (h_g - r)) / L}{1 + \mu h_g / L} \quad (3.18)$$

Equation (3.17) and (3.18) are both used in the case of an all-wheel drive vehicle, while either is dismissed or set to zero in front-wheel or rear-wheel drive scenarios [37].

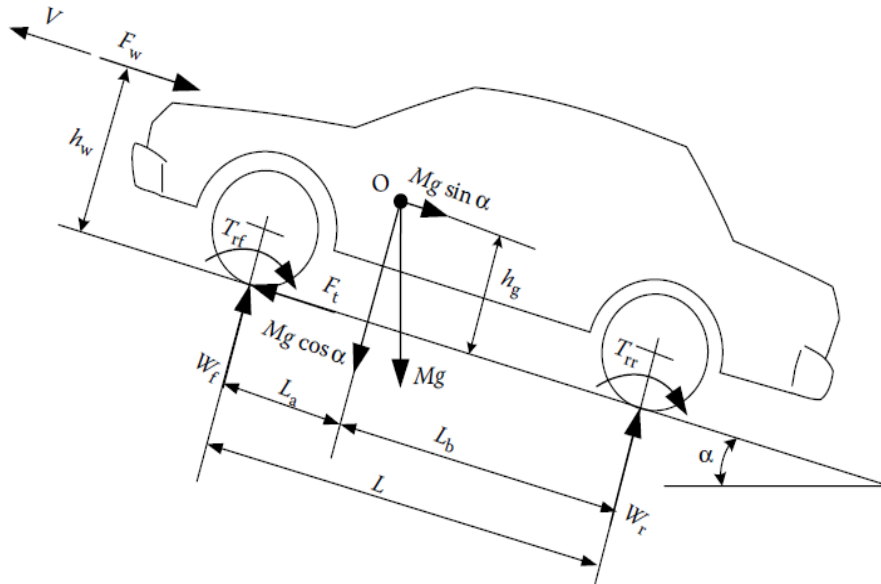


Fig. 3.4. The total forces acting on a two-axle vehicle.

3.2.4 Tire-road model

In general, two approaches were employed to construct the tire model: the analytical approach and the empirical approach [38]. The analytical approach aims to describe the structure of the tire and the characteristics of its deformation by developing the relationship function between back force, tangential force, and other related parameters. For example, Dahl model and LuGre model are using this approach [39]. The empirical approach is to obtain the characteristic relationship function between the tire and the road by regression analysis of the data of an interaction between a large number of tires and road. For example, Pacejka's Magic Formula tire model is widely adopted in the analysis of vehicle dynamics.

According to the purpose of this study, the Magic Formula tire-road model is used to calculate the longitudinal tire forces as the vehicle is running under different road conditions. The expression of the Magic Formula is [40]

$$y = D \sin[C \arctan(Bx - E(Bx - \arctan Bx))] \quad (3.19)$$

with

$$Y(X) = y(x) + S_v \quad (3.20)$$

$$x = X + S_H \quad (3.21)$$

where y represents friction coefficient μ ; x is the slip ratio (λ); B is stiffness factor; C is shape factor; D is peak value; E is curvature factor; S_H is the horizontal shift; S_V is the vertical shift.

According to the different values of parameters B , C , D , E , S_H , and S_V , the different tire-road adhesion model can be obtained, namely the μ - λ curve. These numerical values are based on empirical tire data and typical sets of constant Magic Formula coefficients for common road conditions. Table 3.3 shows the empirical values of parameters under the four common road surfaces. Among parameters, the horizontal

shift and the vertical shift are set to zero. Road 1, 3 will be applied in the following studies. The μ - λ curve of the four different roads is shown in Fig. 3.5.

Table 3.3 The parameters of Magic Formula under four common road surfaces

Road surface	D	B	C	E
1, Dry concrete	0.95	5.5	2.1	0.90
2, Wet concrete	0.80	5.0	2.4	0.96
3, snow	0.4	7.0	2.6	1.00
4, Ice	0.2	10.0	3.0	1.00

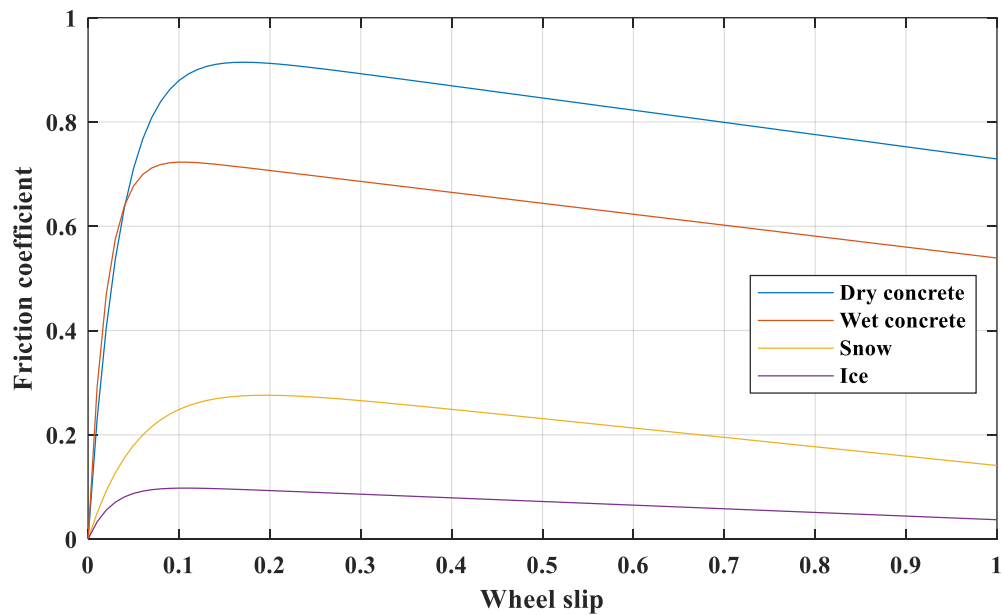


Fig. 3.5. μ - λ curve of the four different roads.

3.2.5 The model of vehicle dynamics

Based on the above discussion, the vehicle dynamics model is built in MATLAB/Simulink environment. The target vehicle is a four-wheel drive electric vehicle with a single gear transmission. The modeling mechanism relies on a quarter-vehicle model. The schematic diagram of the vehicle dynamics model is illustrated in Fig. 3.6, which includes five parts: aerodynamic drag force, rolling resistance force, grade force, acceleration resistance force, wheel slip, and effective traction force. The purpose of the vehicle dynamics model in the proposed system is to simulate the vehicle speed with the input of torque produced by the electric motor. The effect of wheel slip and other road factors, such as road grade and road surface, are considered in this model so that this model makes the proposed system have the ability to simulate the vehicle behavior under different road conditions.

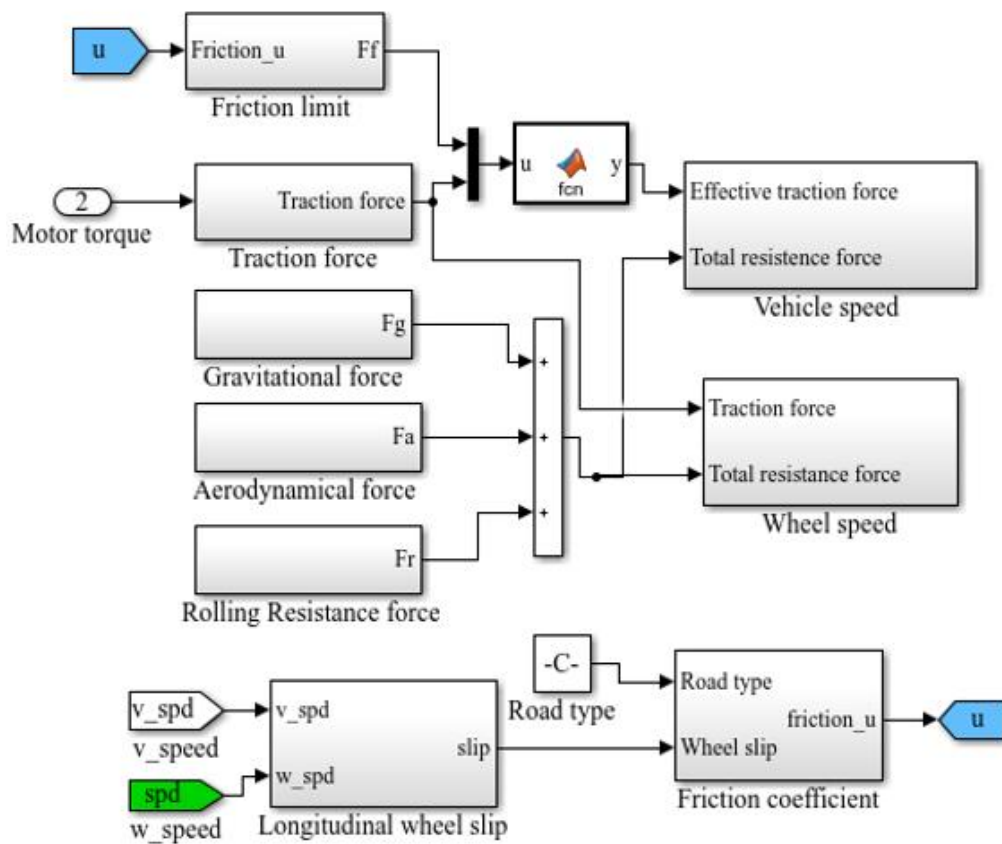


Fig. 3.6. Schematic diagram of the vehicle dynamics model.

3.3 Vehicle load modeling

Here, the vehicle dynamics model and the vehicle load model are convertible for the sake of consistency. The vehicle dynamics model is to input the torque to obtain the target vehicle speed. Vehicle load is to input vehicle speed to obtain required motor torque based on the target vehicle configuration and predefined road conditions. The derivation of the required motor torque for desired vehicle speed is a backward-facing stream of power flow calculation. The details are as follows:

The longitudinal wheel slip λ is considered in this model, and equation (3.11) expresses the relationship between vehicle speed v and wheel speed $r\omega$. The wheel speed ω_w is proportional to the motor speed ω_m , and the relationship through the gear ratio G is expressed in equation (3.22).

$$\omega_w = \frac{1}{G} \omega_m \quad (3.22)$$

The transmission shaft speed ω_t is equal to the motor speed ω_m .

$$\omega_t = \omega_m \quad (3.23)$$

The longitudinal wheel velocity is approximated by $v_w=r\omega_w$, where r is the wheel radius, and hence the longitudinal acceleration a is:

$$a = \frac{1}{G} r \dot{\omega}_m \quad (3.24)$$

The longitudinal vehicle equation is given as:

$$F_a = ma = F_t - F_f - F_g - F_d \quad (3.25)$$

Based on equation (3.24), it can be rewritten as:

$$m \frac{1}{G} r \dot{\omega}_m = F_t - F_f - F_g - F_d \quad (3.26)$$

$$F_t = \frac{1}{G} mr\dot{\omega}_m + F_f + F_g + F_d \quad (3.27)$$

Substituting (3.27) into the equation for wheel rotational dynamics $I_w\dot{\omega}_w = T_w - rF_t$, the torque at the wheels to reach the desired speed is

$$T_w = \frac{1}{G} I_w\dot{\omega}_m + \frac{1}{G} mr^2\dot{\omega}_m + r(F_f + F_g + F_d) \quad (3.28)$$

where T_w is the wheel torque and I_w is the wheel inertia. Substituting (3.28) into the equation for the transmission dynamics which is $I_t\dot{\omega}_t = T_t - \frac{1}{G}T_w$ and with $\omega_t = \omega_m$, the torque on the transmission is

$$T_t = (I_t + I_w \frac{1}{G^2} + m \frac{1}{G^2} r^2)\dot{\omega}_m + \frac{1}{G} r(F_f + F_g + F_d) \quad (3.29)$$

where T_t is the torque on the transmission, and I_t is the inertia of the transmission. Substituting (3.29) into the electric motor dynamics equation which is $I_m\dot{\omega}_m = T_m - T_t$, the torque required on the motor is

$$T_m = J_m\dot{\omega}_m + \frac{1}{G} r(F_f + F_g + F_d) \quad (3.10)$$

where, $J_m = I_m + I_t + (I_w + mr^2) \frac{1}{G^2}$ which is the effective inertia reflected on the motor side.

The structure of the vehicle load is shown in Fig. 3.7. To verify that the two models are convertible, set a standard drive cycle (UDDS) as input to the vehicle load model, then send the required torque to the vehicle dynamics to obtain the vehicle speed. The related parameters are shown in Appendix II and the electric vehicle is driving on the flat dry concrete road. The effect of wind speed is neglected. The schematic of the verification is shown in Fig. 3.8. If the reference speed matches the simulation speed, the

two models are convertible, vice versa. The result (showing in Fig. 3.9) indicates the two speeds are perfectly matching. Fig. 3.10 shows the required driving torque from the electric motor based on UDDS. The maximum required motor torque is 140.3 Nm and the maximum torque of the selected PM motor is 160 Nm. Therefore, the PM motor meets this operation requirement.

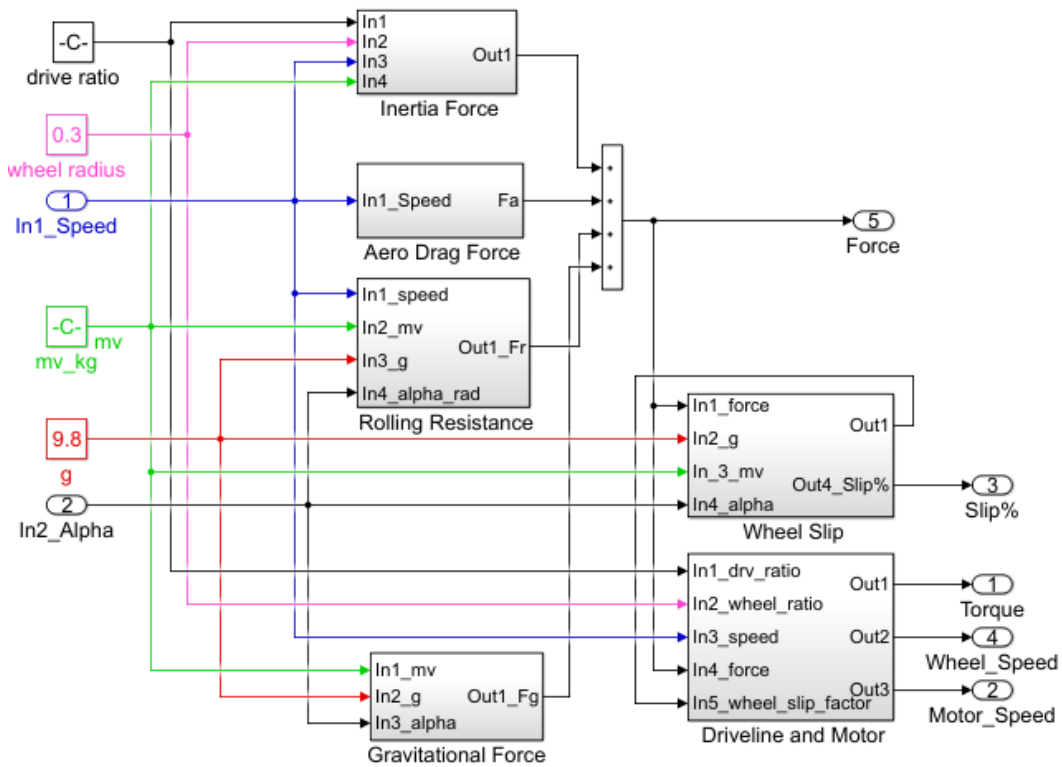


Fig. 3.7. Schematic of vehicle load.

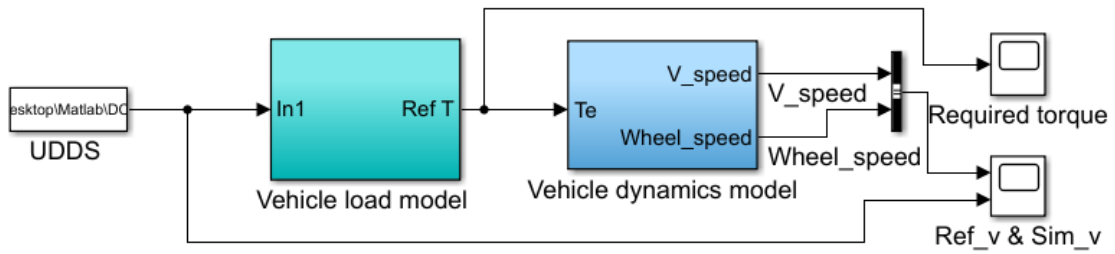


Fig. 3.8. Schematic of verification of vehicle load model.

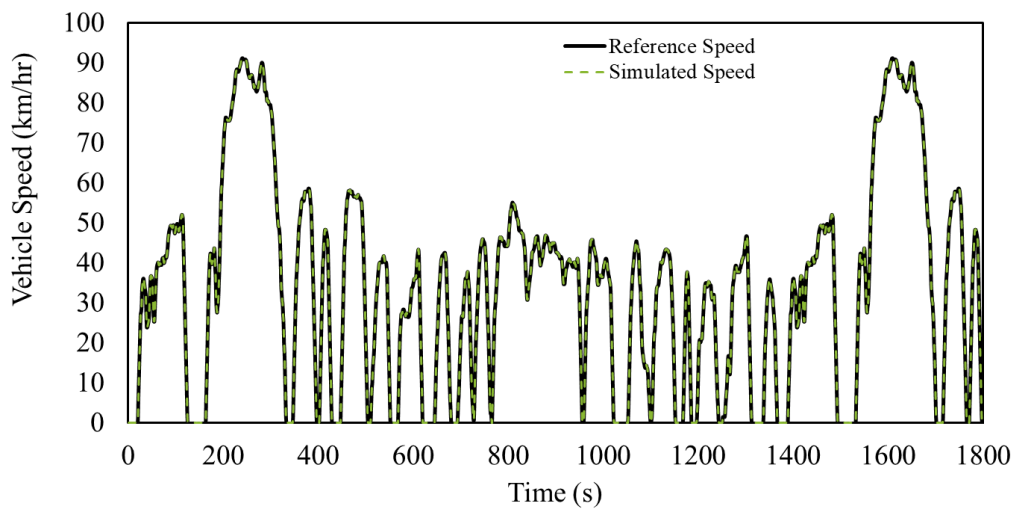


Fig. 3.9. Verification results of vehicle load model.

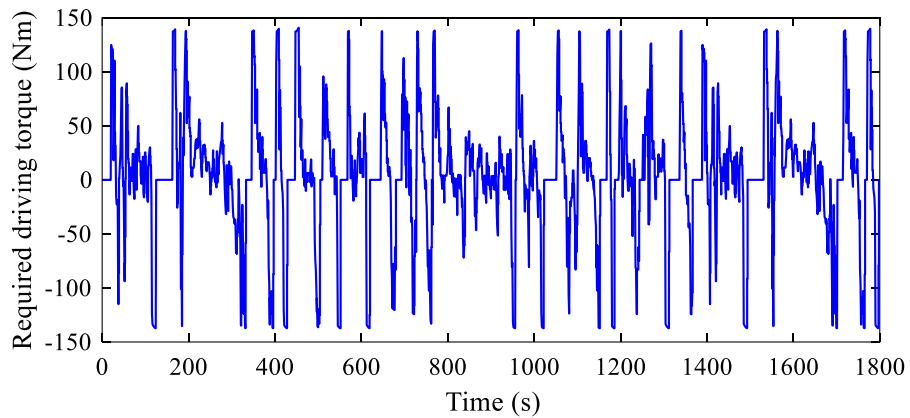


Fig. 3.10. The required driving torque based on UDDS.

3.4 Verification of simulation model

In most cases, the results obtained from one method of simulation should be validated by other known methods to verify the effectiveness and correctness of the results. To validate the results obtained from the Matlab/Simulink simulation model, a vehicle with the same parameters as those provided in Appendix II was designed and simulated in ADvanced Vehicle SimulatOR (ADVISOR). The results of the required PMSM motor torque obtained from ADVISOR were compared to the results of the torque generated by the vehicle load simulation model. Fig. 3.11 shows the comparison between the torque simulated in ADVISOR and the torque obtained from the Matlab/Simulink model.

Fig. 3.11 demonstrated that the torque generated by ADVISOR and Matlab/Simulink closely follow the same path. Slight mismatches exist, however, due to the involvement of the electric motor and powertrain control in ADVISOR model. Additionally, observable differences exist in the negative torque values where the electric motor absorbs energy, and the vehicle applies regenerative braking [41]. The reason is that in a real vehicle operating in regenerative braking mode, only part of the energy can be absorbed by the electric motor, and the rest is wasted through mechanical brakes. As a result, ADVISOR sets braking limitations, which is not the case for the proposed model because mechanical brakes are not considered.

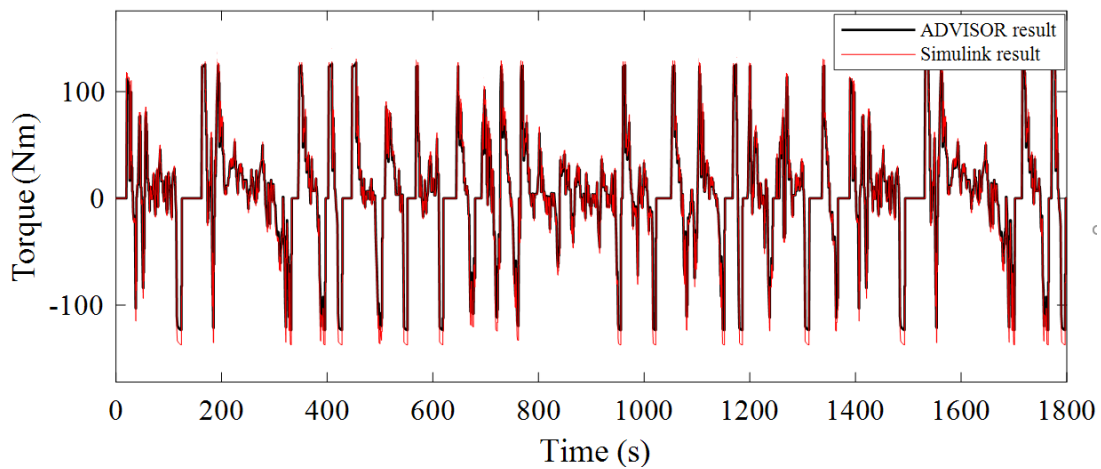


Fig. 3.11. The required torque comparison between ADVISOR and the Simulink model.

4 FUZZY LOGIC BASED WHEEL SLIP CONTROL

4.1 Introduction to wheel slip control

In vehicle dynamics, wheel slip is the relative motion between a wheel and a road surface that the vehicle is running on. Wheel slip can be generated either by the wheel's rotational speed being greater or less than the free-rolling speed, or by the wheel's plane of rotation being at an angle to its motion direction. Regarding the direction of wheel slip, wheel slip is classified into two types: longitudinal slip and lateral slip. Longitudinal slip affects acceleration and braking performance of the vehicle, while the lateral slip is associated with stability and controllability of the vehicle [42]. The object of this work is to study the dynamic performance of a PMSM motor as the traction motor of the electric vehicle in terms of power flow - here only longitudinal slip is considered, and lateral slip is neglected.

Typically, the adhesion control between the wheel and the road has been classified into two types of driving assistant systems: the traction control (TC), involved during acceleration, and the antilock braking system (ABS), enabling deceleration. Both are using the same mechanism to control the wheel slip to maintain the friction coefficient close to the optimal value as possible. The motivation for introducing the wheel slip control in this study is to empower the proposed system with the ability, to test the PMSM motor performance when the vehicle is running over slippery surfaces, such as snow or ice. Without the slip control in these conditions, the driver model may employ excessive wheel torque to achieve the desired vehicle speed in a skid (braking) or high wheel spin (acceleration) situation. The responsibility of the slip control is to avoid such pernicious operation by reducing the torque requested by the driver, to a level where the longitudinal wheel force is maximized, and the slip rate is kept in a safe and optimal range [43], [44].

4.2 Control algorithms of wheel slip

With the development of automatic control system, electronic technology, and the increasing demand in handling stability and safety of a vehicle, the anti-skid control of the vehicle is also becoming more precise and effective, with simplified structure, sensitive response, and more diversified control strategies. At present, the ruling control theory methods include logic threshold control [45], PID control [46], optimal control [47], [48], [49] sliding mode variable structure control [50], [51], fuzzy logic control [52], [53], and neural network control [54], [55]. In this section, five control methods are introduced briefly, and the suitable control method for this study is selected.

4.2.1 Logic threshold control

This method is currently the most widely used control method in the anti-skid control of an automobile, and its working principle is to set a threshold value as the control threshold of the control target variable in advance. When the control target variable crosses this gate threshold, the control system responds immediately accordingly to adjust the other variables. For the vehicle-driven anti-skid control, the threshold value of the wheel slip rate is set according to an empirical value first; then the system compares the detected real-time slip rate of the wheel with the threshold value. Therefore, the principle and structure of this control method are very simple, without the specific mathematical model of the controlled object. The computing load of the system is small, and the relative response is fast. The biggest drawback is that the wheel's target slip rate (threshold) needs to be obtained empirically. For a vehicle with real-time dynamic changes and strong time-domain and complex road conditions, the threshold value is difficult to get, plus the control accuracy is not enough because of high fluctuations and poor stability. Meanwhile, due to the large degree of dependence of the threshold value on experience, the lack of comprehensive consideration of different vehicle models, ground conditions and particular operation states, its generality and robustness are poor.

4.2.2 PID control

PID control is based on classical control theory and has developed very maturely as a control technology for continuous systems. The advantage of this method is that it does not need to fully understand the mathematical model of the controlled object in advance. Instead, it only needs to adjust the parameters of the regulator according to experience. It has very sensitive and fast response to changes in the parameters of the controlled object. Because of the simple control structure, it is the most widely used control technology at present. The fundamental principle of PID control is to make a certain logic operation of the error that formed between the real-time observed value of the controlled object and the observed value of the target, then use the result as the input of the judgment of control instructions. The diagram of Fig. 4.1 shows the working principle of PID control. The control functions are expressed mathematically as

$$e(t) = r(t) - y(t) \quad (4.1)$$

$$u(t) = K_p \left[e(t) + \frac{1}{T_i} \int_0^t e(t) dt + T_d \frac{de(t)}{dt} \right] \quad (4.2)$$

where K_p denotes the coefficient for the proportional term, T_i denotes the integration time, T_d denotes the derivative time.

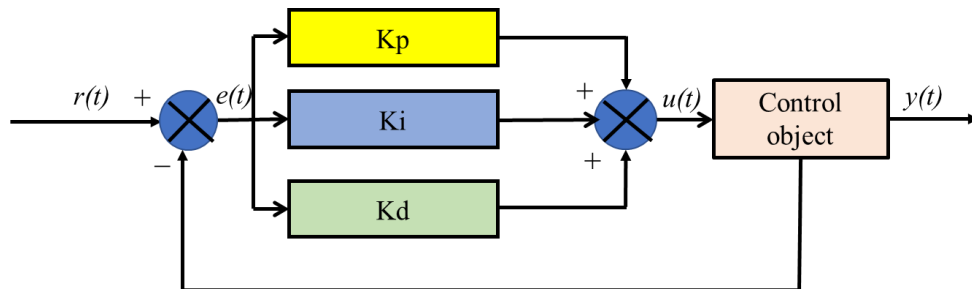


Fig. 4.1. PID control diagram.

PID control is a simple linear control algorithm. For traditional traction and anti-lock braking control, it is usual to observe the error between the real-time wheel slip and target slip as the input value of the system control. Then, the control system adjusts the

output traction torque or the output braking torque according to the magnitude of this value, to control the actual wheel slip rate within the target one. Its easy implementation and maintenance benefits from the relatively simple structure. Since PID control depends on the mathematical model of the control object and requires parameters analysis and tuning, it is more accurate and stable than the logic threshold control. On the other hand, it also has some limitations. For the very complicated nonlinear system of vehicle motion, it is difficult to build up the mathematical model and tune the parameters. That is the main reason that it is hard to achieve high control accuracy in practical applications.

4.2.3 Sliding mode variable structure control

Variable structure systems are a type of systems by means of which the control laws are purposely changed by some characterized rules, which rely upon the state or execution of the system. Sliding mode control is a specific kind of factor structure system intended to drive and after that oblige the system state to exist in an area of the switching function. The fundamental difference between this control strategy and conventional control lies in the discontinuity of control, namely, the switching behavior of a system's "structure" over time. The control feature is to constrain the system to move up and down with small amplitude and high frequency along the specified track of state under the certain characteristic, so-called "sliding mode" motion. This sliding mode can be designed without regard to system parameters and disturbances, so it has good robustness. The basic concept of a variable structure system can be described in a mathematical expression [56], [57]:

$$\begin{cases} \dot{x}_1 = x_2 \\ \dot{x}_2 = f(x) + g(x) \cdot u(t) \end{cases} \quad (4.3)$$

where x_1 represents the control variable. Generally, if the tracking trajectory is x_d , then the tracking error is defined as $e = x_1 - x_d$. The dynamic characteristics are determined by a sliding surface $m(t) = 0$. In the actual control process, the "sliding mode" movement is carried out back and forth along the cutting plane by setting up a

discontinuous control switch: $u = \begin{cases} u^+, m > 0 \\ u^-, m < 0 \end{cases}$. Then, the control variable reaches the trace point (termination point) x_d . For the conventional vehicle anti-slip control system, the wheel slip ratio is usually used as the control target, and the optimal slip ratio (λ) is set as the value of the tracking trajectory. Therefore, the tracking error is $e = \lambda - \lambda_o$, and the switching function is

$$m_{(t)} = C_1 e + \dot{e} = \dot{\lambda} + C_1(\lambda - \lambda_o) \quad (4.4)$$

Neglecting the rolling assistance and aerodynamic drag force, the simplified vehicle dynamic equations are as below:

$$\begin{cases} m\dot{v} = \mu N \\ J\dot{w} = T - \mu N r \end{cases} \quad (4.5)$$

where J is the wheel inertia, r is the radius of the wheel, v is the longitudinal vehicle speed, w is the wheel angular speed, N is the vertical load of the vehicle, and T is the driving torque. Usually, the torque of the drive wheels, which is the torque provided by the powertrain for accelerating or braking, is set as the control volume and controlled by the discontinuous control switch. The control principle diagram as shown in Fig. 4.2

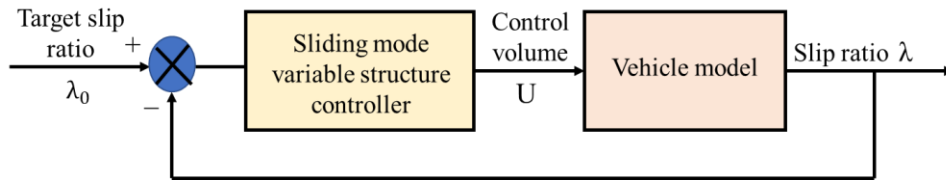


Fig. 4.2. The diagram of sliding mode variable structure control.

Since the sliding model can be designed according to the actual situation and is not sensitive to the change of parameters and the response of external interference, it has good anti-interference ability and self-adaptability. However, it also has a predominant drawback - it is difficult to control variables correspondingly fixed at the equilibrium point and fluctuation near the sliding mode surface leads to system jitter. The demerit is

very unfavorable for adjusting the wheel hub motor torque. Therefore, this method does not have good applicability for anti-slip control in the wheel hub motor vehicle.

4.2.4 Neural network control

It is a control algorithm to simulate the recognition and discrimination of the human brain and is also a complicated non-linear control technology. It mainly imitates the dynamic process of the neural network. The learning process and running process are conducted by learning certain control rules to cope with the input signal accordingly. Its core idea is to use the network to realize the mapping relationship between input variables and output variables. It has good associativity, parallelism and self-learning ability, and the control does not require an accurate mathematical model, and often can be combined with a fuzzy logic control strategy, which makes full use of the learning ability of neural network to design reasonable and practical fuzzy control rules with fast and efficient fuzzification and de-fuzzification. This control strategy has a complex control algorithm structure and insufficient system accuracy, so it has not been widely used in practical application

4.2.5 Fuzzy logic control

It is an intelligent control method that imitates the thought process of the human brain. Based on the conceptual fuzzy set and fuzzy mathematical logic computation, the designed control strategy can be carried out accordingly by intellectual control by a computer, which has a certain degree of adaptability to system parameter changes, and strong robustness. Also, since its algorithm structure is relatively simple and has fast system response, it is very suitable for applications featuring with the fast time-varying dynamic system, such as automotive systems. Due to its excellent adaptability, popularity and intelligence, it is also often applied in many fields such as the chemical industry, humanities, economy, and engineering.

Fuzzy logic control usually only needs the accurate mathematical model of the control object. Consequently, its control structure is simple in design, and the system is not particularly sensitive to the change of input parameters and external disturbances, so it has good adaptability to nonlinear and time-varying systems. The vehicle itself and its movement are both extremely complex and time-varying nonlinear system, and fuzzy logic control method is very suitable for studying the anti-slip control of the automobile. The schematic diagram of a fuzzy logic control strategy is shown in Fig. 4.3

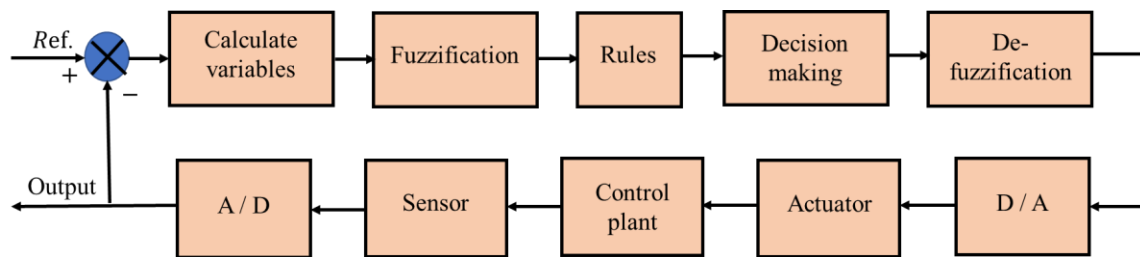


Fig. 4.3. Principle block diagram of fuzzy logic control.

For fuzzy logic based anti-slip control system, the system variables consist of wheel speed, acceleration, and slip rate. Though establishing corresponding fuzzy logic control rules, the output of the driving/braking torque is adjusted timely to reduce the wheel slip. Meanwhile, this method can also be applied to solve the problem of road surface recognition. According to the relationship between the road surface adhesion coefficient and the wheel slip rate, a knowledge rule base of typical road conditions can be established, and the optimal slip rate of the vehicle under the current road conditions can be calculated though fuzzy logic inference.

In the actual operation of a vehicle, the wheel slip state is non-linear and a dynamic process with rapid change. Because there are so many parameters involved in wheel slip control, it is impossible to calculate the real-time data accurately and statistically. Therefore, for slip control, it is necessary to choose a simple algorithm structure, fast system response, and high sensitivity and good robust control strategy.

Based on the above analysis, it can be seen that the fuzzy logic-based control strategy is the most appropriate in this study. According to the actual slip condition of the wheels, the degree of slipping is graded in a certain range, and then the appropriate motor output torque is adopted to improve the slip condition of the wheels contraposing the different levels, eventually controlling the wheel slip and avoiding skidding.

In the previous research on the control strategy of anti-slip control, some of them introduced the road surface recognition system, which is by establishing a road surface observer to predict the road surface adhesion conditions and then calculate the wheel slip rate, and through fuzzy calculation to carry on the preliminary judgment. Therefore, there are two times of fuzzy calculation in the practical application, which reduces the control accuracy dramatically. In this study, the wheel slip rate is directly chosen as the control object in fuzzy logic-based slip control with given the road conditions, and the wheel slip state is judged depending on wheel dynamic and vehicle dynamic.

4.3 Fuzzy logic-based wheel slip control

4.3.1 Overview of Fuzzy logic control

Fuzzy logic control is an emerging control technology based on fuzzy mathematics theory and its core is to imitate human brain thinking by mathematical methods; to identify, measure, fuzzy, fuzzy implicate (inference), fuzzy control, precision, make decisions. That is using precise means and fuzzy methods to deal with complex things, and ultimately form effective control. Fuzzy control mainly includes the following concepts:

Fuzzy sets: The general term for a study object that has certain properties is called a fuzzy set, which reflects the characteristics of some aspects of the research object and the degree of commonality between them. In general, the sets are described in the following three ways:

- Enumeration method: enumerate the elements one by one which is qualified for a set

- Definition: not enumerate the object of the study one by one but list the elements that have the common characteristic to constitute a set.
- Characteristics of function notation: use the explicit boundary of classical set theory to separate the set.

For many complicated objects, if using a precise method to address the problems, it proves to be very difficult and has low feasibility. Therefore, the concept of fuzzy sets is introduced which the objects can be classified into the same category as long as they contain a degree of relevance. Namely, its connotation and extension are expanded, which can be a fuzzy quantity.

Membership function: For a fuzzy object that can not be identified by its properties or defined by the exact values of ordinary mathematical theory (such as 0 or 1), in order to illustrate its properties in some degree, a relative range value is introduced to describe it, such as the range between 0 and 1, to define its properties in the interval [0,1]. In general, the conceptual precise value can be converted into an infinite number of possible fuzzy logic values. The membership function is usually expressed by $u_A(x)$, in which A represents set A and x represents the elements of set A . In the above example, the function can be expressed as: $0 \leq u_A(x) \leq 1$. This is the membership function that can effectively describe the characteristics of fuzzy sets.

The method of determination of membership function: The membership function establishes the rules mainly through practical experience. The commonly used determination methods include the statistical method, analytical method, relative selection method, filter function method, variable model method, demonstration method and subset comparison method [58]. Different from the frequency statistic of certain events in random statistics, fuzzy statistics describe the degree of relevance of fuzzy events, and the result is called the membership degree.

Fuzzy logic: It is actually a tool and method for describing and analyzing complex or uncertain things by imitating the way of thinking of the human brain. Although the fuzzy control is called “fuzzy”, in the whole logic control process, each defined input element corresponds to a certain output, and even these outputs can be

predicted. Therefore, fuzzy control is not “fuzzy”, it is an effective control method to solve imprecise or overly complicated problems in a precise way.

The formation of these fuzzy concepts and theories has created the conditions for the birth of fuzzy controllers. The basic components of the fuzzy control system can be represented in Fig. 4.4.

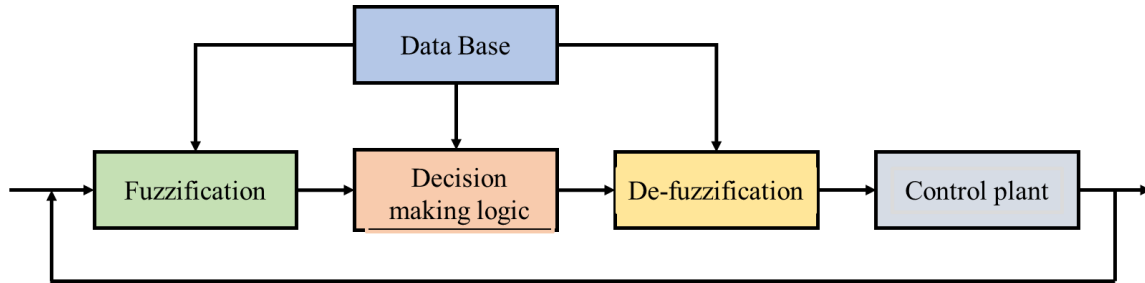


Fig. 4.4. The basic components of the fuzzy control system.

It can be seen from the figure above that the fuzzy controller mainly consists of three core parts: the fuzzification of the input quantity, the fuzzy inference according to the fuzzy control rules and the de-fuzzification. The specific process is as follows: Firstly, 1) compare the reference value (input) of the system with the feedback value to analyze the error; 2) determine the error rate of change and fuzzify the input value; 3) conduct fuzzy inference to fuzzified input signal according to fuzzy rules; and 4) convert the reasoning result into precise control quantity to form precise control.

4.3.2 Development of fuzzy logic controller based on optimal wheel slip ratio

The development of fuzzy logic controller is to define the structures of input, output, and fuzzy control rules. It mainly has three steps: fuzzification, fuzzy control rules, and defuzzification. The structures of input and output of fuzzy controller have two forms: SISO (single input/output) and MIMO (multiple inputs/outputs). For the vehicle’s traction/ antilock braking control, there is generally only one input, which is wheel slip

ratio. In order to make the control more accurate, often the rate of change of wheel slip ratio and slip ratio is taken as the input, and the motor torque is taken as the output. For optimal wheel slip ratio control, first pre-set an ideal slip ratio λ_0 ; then calculate the error of slip ratio between the ideal value and the actual one λ , namely $E = \lambda - \lambda_0$, and the rate of change of error $\Delta E = dE/dt$; take the change of the motor torque U as the output. The block diagram of fuzzy logic based wheel slip control is shown in Fig. 4.5.

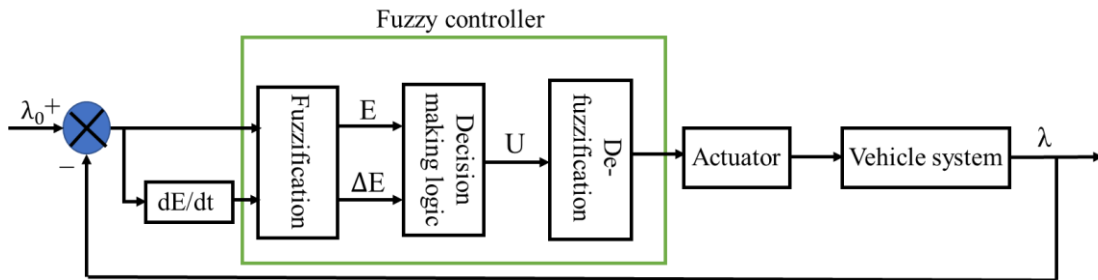


Fig. 4.5. The block diagram of fuzzy logic based wheel slip control.

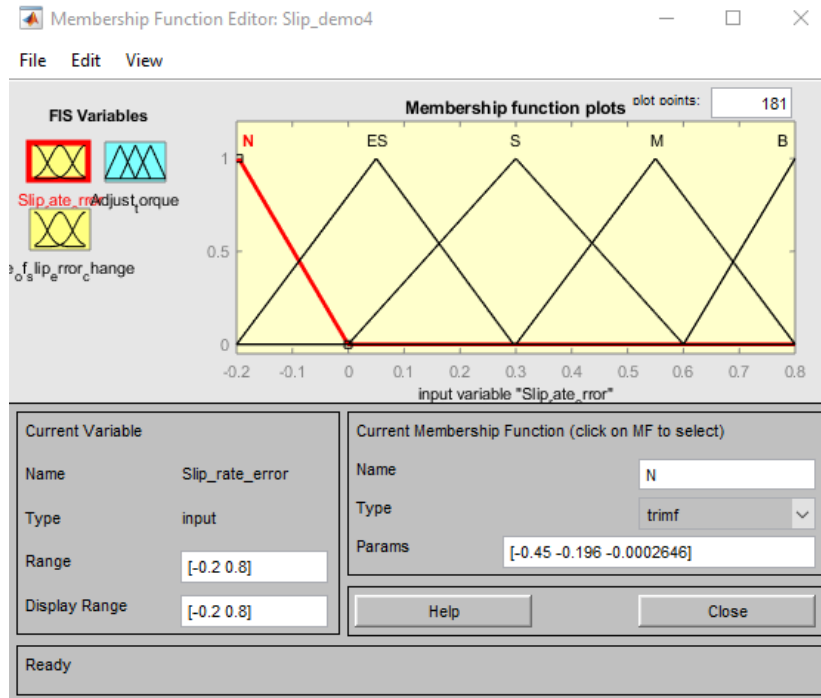
- Fuzzification: The controller accepts two inputs, error E and the rate of change of error ΔE . The range of wheel slip is $[0,1]$, so the physical domain of E is $[-0.2, 0.8]$. With the quantization factor $K_e=1$, the error E is mapped on fuzzy sets with a universe of discourse ranging from -0.2 to 0.8 . Generally, the physical domain of ΔE is $[-50, 50]$ [59], [60]. With the quantization factor $K_{es}=0.02$, the rate of change of error ΔE is mapped on fuzzy sets with a universe of discourse ranging from -1 to 1 . The output of adjust torque U is mapped on fuzzy sets with a universe of discourse ranging from -2 to 10 . Similarly, the physical domain of the output, the adjust torque of motor, is $[-50, 250]$, and usually the quantization factor K_u is set as 0.01 [61], [62].

The fuzzy membership functions are showing in Fig. 4.6, and the summarized input and fuzzy output sets are as follows:

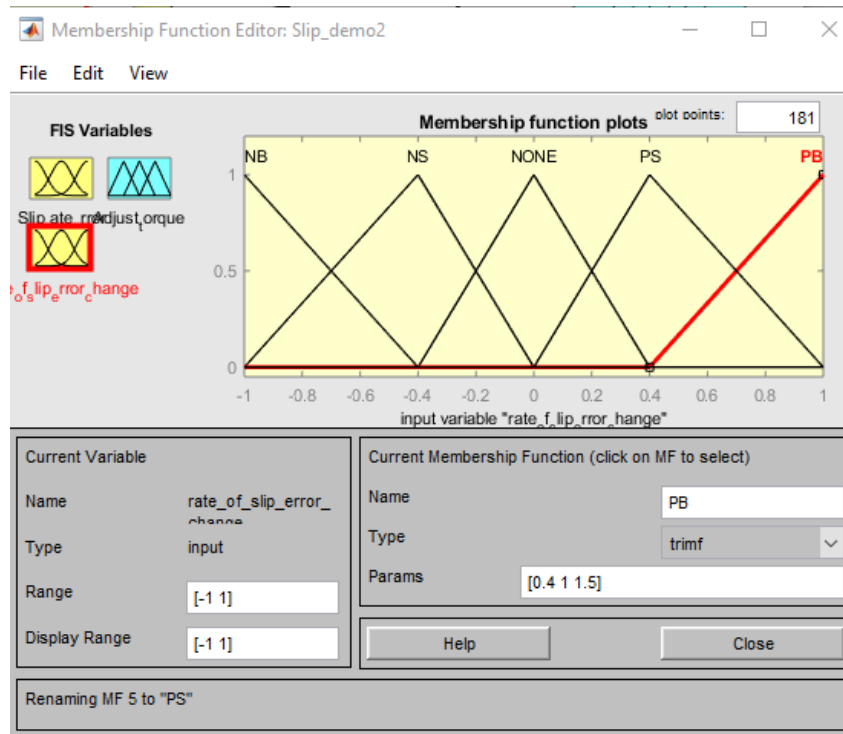
Wheel slip ratio deviation: $E = [N, ES, S, M, B]$;

The change rate of E : $\Delta E = [NB, NS, NONE, PS, PB]$;

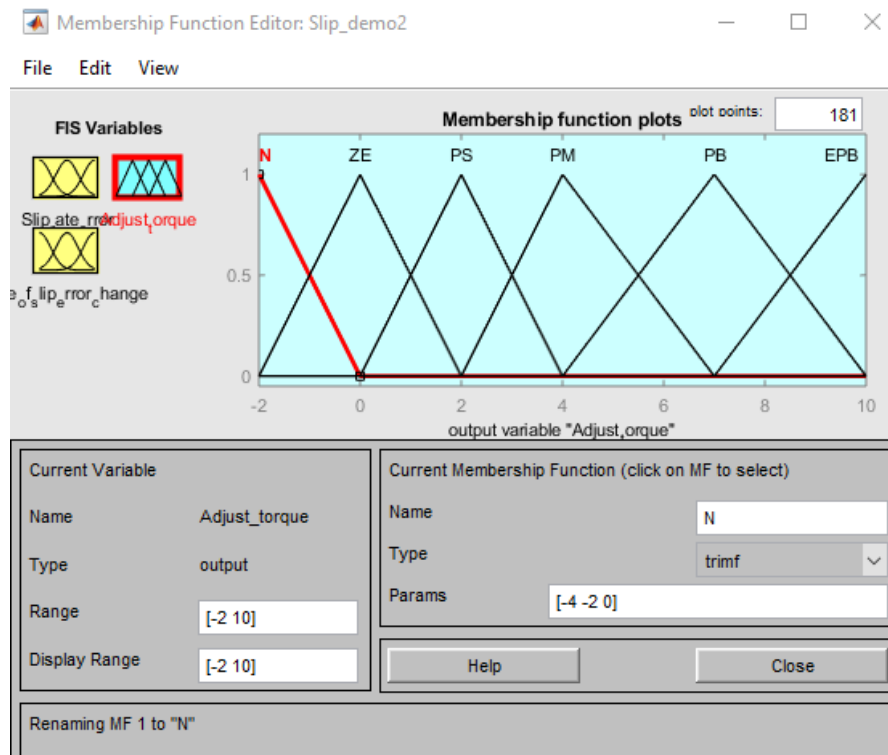
Output (adjust torque): $U = [N, ZE, PS, PM, PB, EPB];$



(a)



(b)



(c)

Fig. 4.6. Fuzzy membership functions: (a) input error; (b) error change rate; (c) adjust torque.

Note: N is negative in fuzzy domain E; ES is extremely small in fuzzy domain E; S is small in fuzzy domain E; M is middle in fuzzy domain E; B is big in fuzzy domain E; NB is negative in fuzzy domain ΔE ; output N is negative in fuzzy domain U; PS is small in fuzzy domain U; PM is middle in fuzzy domain U; PB is big in fuzzy domain U; EPB is extremely big in fuzzy domain U.

- Fuzzy control rules: The fuzzified inputs are fed to the fuzzy control rule base that determines the corresponding wheel slip state on given input data and generates a fuzzy output in terms of torque change ΔT . The fuzzy control rules are built based on the Mamdani fuzzy inference system. The decisions of the fuzzy control rule

base are based on a set of 25 rules for the 2-input fuzzy system, shown in Table 4.1. The rules are *if-then* statements that determine the corresponding output adjust torque response for a given input condition to maintain the optimal wheel slip. For example, if E is PB and the ΔE is PS, it depicts that the wheel speed is much bigger than vehicle speed. Therefore, the traction torque should decrease significantly. Once the inference engine triggers the related rules for the given inputs, the weight of the adjust torque is computed from the membership functions. The rule base was created using human experience and then refined with trial and error. 3D curve representation of the rule base is shown in Fig. 4.7. The sharp outer edges of the curve show the ability to make drastic changes in the torque command.

Table 4.1 Fuzzy rule base

$\Delta E \backslash E$	N	ES	S	M	B
NB	N	N	ZE	PS	PS
NS	N	ZE	PS	PS	PM
NON	N	PS	PS	PM	PB
PS	PS	PM	PM	PB	PB
PB	N	PS	PS	PB	EPB

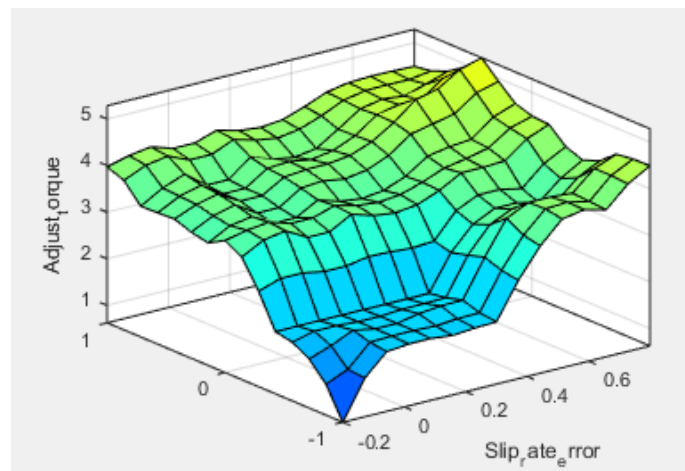


Fig. 4.7. 3D representation of fuzzy rule base.

- **Defuzzification:** The weighted output is transformed into adjusted torque signal through defuzzification. This is accomplished by the inverse transformation to map the adjust output from the fuzzy domain to a crisp real-time value. A common and useful method of defuzzification is the center of gravity (COG) [63], which calculates the center of gravity of the area under the membership function representing the output fuzzy term. The output, u , is given by:

$$u = \frac{\sum_{i=1}^n x_i \mu(x_i)}{\sum_{i=1}^n \mu(x_i)} \quad (4.6)$$

where n is the number of rules; x_i is a point in the universe of discourse and $\mu(x_i)$ is the weight of i th rule. The effective output of the fuzzy controller is the amount of adjusting motor torque, ΔT ; it is integrated to the dyno controller to generate the command torque. This fuzzy-based control algorithm was implemented in the Fuzzy Toolbox of MATLAB/Simulink. The toolbox enables the user to build multiple inputs and outputs, to define the rule base in linguistic terms in the Rule Base Editor. It is also capable of displaying which rules are triggered for any given set of inputs to indicate the resulting output generated.

4.3.3 Wheel slip ratio calculation

The determination of wheel slip ratio is essential to implement the fuzzy logic control based on optimal wheel slip ratio. According to equation (3.11), wheel slip ratio is associated with the vehicle speed v and the wheel speed ωr . A quarter mass of the vehicle model for both vehicle dynamic and wheel dynamic is used to obtain v and ωr .

Vehicle dynamic: According to Newton's second law, the motion of the vehicle on longitudinal direction is

$$ma = F_{et} - F_f - F_g - F_d \quad (4.7)$$

where F_{et} denotes the effective traction force, F_f denotes the rolling resistance force, F_g denotes the gravitational force, F_d denotes aerodynamic drag force. Based on the acceleration of the vehicle, the vehicle speed is

$$v = \int a dt \quad (4.8)$$

Wheel dynamic: For the driving wheel, the balance of moments on the wheel is

$$\begin{cases} J \frac{d\omega}{dt} = T_t - T_{x2} - T_{f2} \\ T_{x2} = F_{x2}r \end{cases} \quad (4.9)$$

Where J represents the equivalent rotational inertia on the wheel side; T_t represents the traction torque from the motor; T_{x2} , F_{x2} represents the reactive torque and force of the tangential force from the ground to the wheel respectively; and T_{f2} represents the wheel rolling resistance torque. Fig. 4.8 shows the force analysis of the driving wheel. F_{x2} can be calculated based on equation (3.10) and (3.19).

Drawing upon the knowledge of the kinetic energy theorem of theoretical mechanics, the total kinetic energy of the equivalent unit is equal to the sum of kinetic energies of each component.

$$\frac{1}{2} J \omega^2 = \sum \frac{1}{2} J_s \omega_s^2 \quad (4.8)$$

Where J_s is the moment of inertia of each rotating component; ω_s is the angular speed of each rotating component.

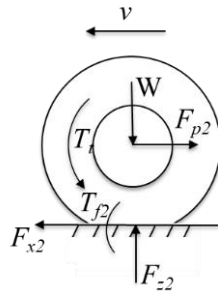


Fig. 4.8 Stress analysis of the driving wheel

4.3.4 PM motor testing environment with fuzzy logic-based wheel slip control

The purpose of integrating the wheel slip control into the electric motor testing system is to simulate the electric vehicle driving on the slippery road. The overall process of PM motor testing environment simulation is illustrated in Fig. 4.10, including driver model, test motor drive model, dyno drive model, vehicle dynamics model, vehicle loads model, fuzzy logic control model. For the sake of simplicity, the same PMSM model is adopted in both the test motor and dyno motor, as discussed in chapter 2. The detailed information about vehicle dynamics model and vehicle loads model are discussed in chapter 3. The driver model is a decision-making module that is designed to decide the acceleration rate and the reference torque applied to the test motor. As shown in Fig. 4.9, a proportional-integral (PI) controller is employed to simulate driver model, where the input is the error between the desired vehicle speed and the simulated speed, and the output is the torque applied to the test motor.

The proposed simulation model is composed of forward and backward vehicle simulation according to the characteristics of the test bench with two electric motors. In section one, the drive cycle provides the desired vehicle speed to driver model; then the driver model generates accelerating or braking signal and sends to the test motor drive. The vehicle dynamics model simulates the vehicle speed based on the traction torque delivered from the test motor drive, and the simulated vehicle speed is fed back to driver model lastly. The whole process emulates driving a vehicle. In section two, the drive cycle sends the desired vehicle speed to vehicle load model to predefine the required motor torque. According to the torque command from vehicle loads, the dyno drive adds load on the test motor. In section three, when the wheel slip ratio exceeds the optimal slip ratio, the fuzzy logic controller adjusts the command torque to the dyno motor. The output torque of the test motor is adjusted to control the wheel slip state.

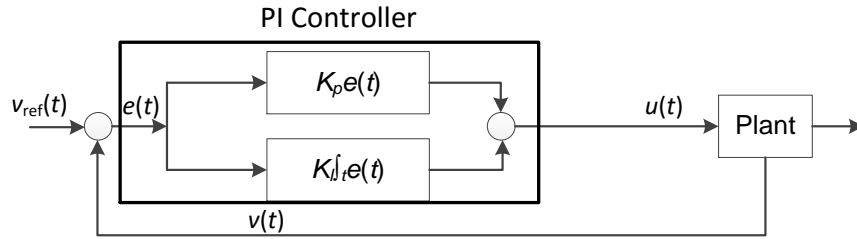


Fig. 4.9. The PI controller-based driver model.

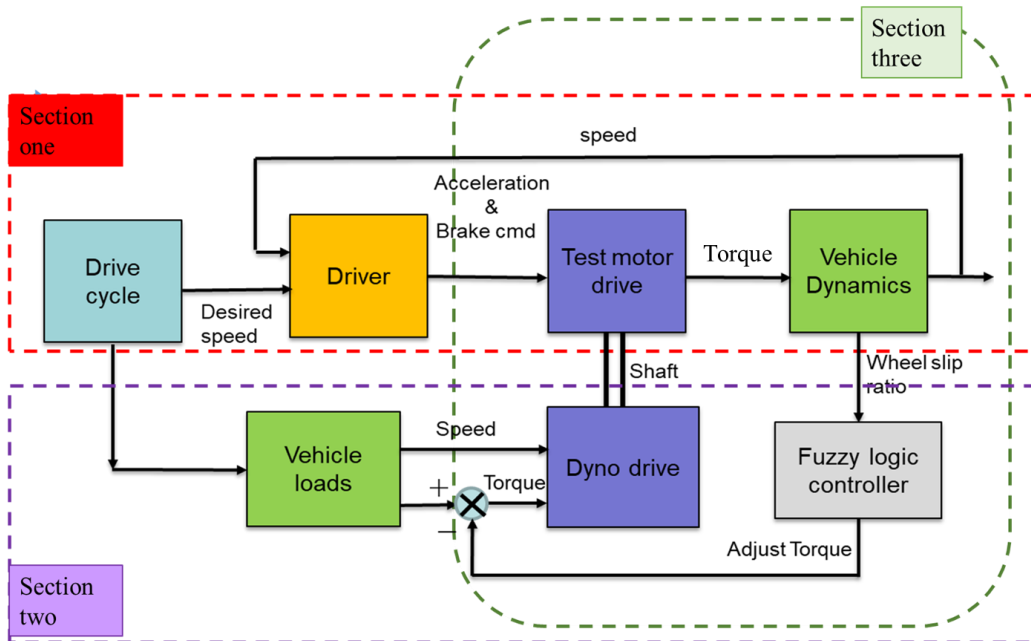


Fig. 4.10. The overall structure of PM motor testing environment simulation.

4.4 Simulation results and analysis

The drive cycle is defined as a series of data points representing the speed of a vehicle versus time. The drive cycles can be utilized to assess the performance of vehicles in various ways. Another use for drive cycles is in vehicle simulations. More specifically, they are used in propulsion system simulations to predict the performance of powertrain components and systems. The United States Environmental Protection Agency provides a number of standard driving schedules such as the Urban

Dynamometer Driving Schedule (UDDS), the Highway Fuel Economy Driving Schedule (HWFET), and more. In this study, UDDS & HWFET is selected as driving requirements to analyze the speed traction performance of the PM motor under the dry concrete road surface and snow road surface.

4.4.1 UDDS test under the dry concrete road condition

UDDS represents the city driving conditions. The analysis of the PM motor operating conditions based on driving cycle is to identify the capability of the PM motor for EV application. Based on the target electric vehicle model, the required torque-speed operation points for UDDS driving condition is obtained as driving the vehicle on the dry concrete road, shown in Fig. 4.11. The yellow dots demonstrate the required operation points for the PM motor; the blue lines and purple lines show the peak torque-speed curve and rated torque-speed curve. The results show that the PM motor has the capability of delivering the torque-speed operation points for UDDS. Moreover, the main operation points are a location in the rated torque-speed realm, which is usually the high-efficiency region of the motor.

Fig. 4.12 (a) shows the speed tracking characteristics of the vehicle employing the PM motor for UDDS. Wheel speed is subject to the speed and output torque of PM motor, and the vehicle speed is affected by the road conditions. The simulated wheel speed is very close to the reference with a subtle difference existing, as presented in Fig. 4.12 (b) during the period of 200 s-320 s. The optimal friction coefficient of the dry concrete road is 0.9 according to Fig. 3.5. So that actual vehicle speed is slightly lower than the wheel speed, as shown in Fig. 4.13. The power of the PM motor under UDDS illustrated in Fig. 4.14, includes the output power consumed to accelerate the vehicle speed, and the generated power as the vehicle decelerates. In practice, there is less generated power during the braking process due to the involvement of mechanical braking system in the vehicle. Most of the driving time, the PM motor is working around rated power (24 kW). From the simulation results, the PM motor can drive the vehicle in urban driving conditions.

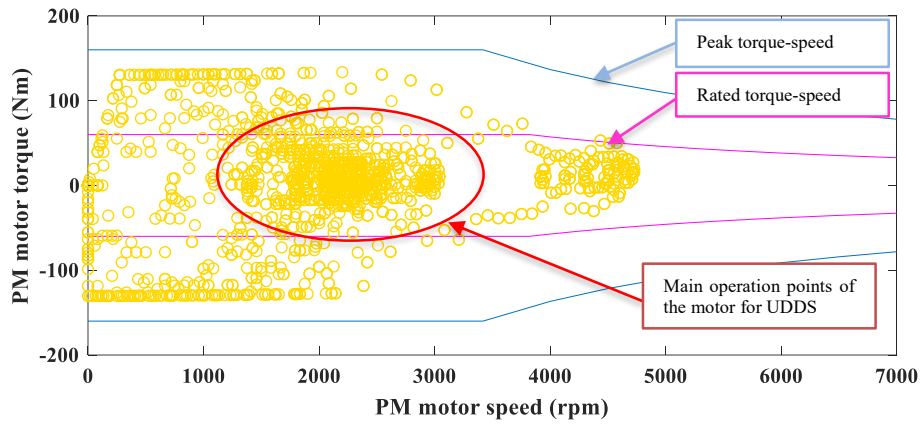
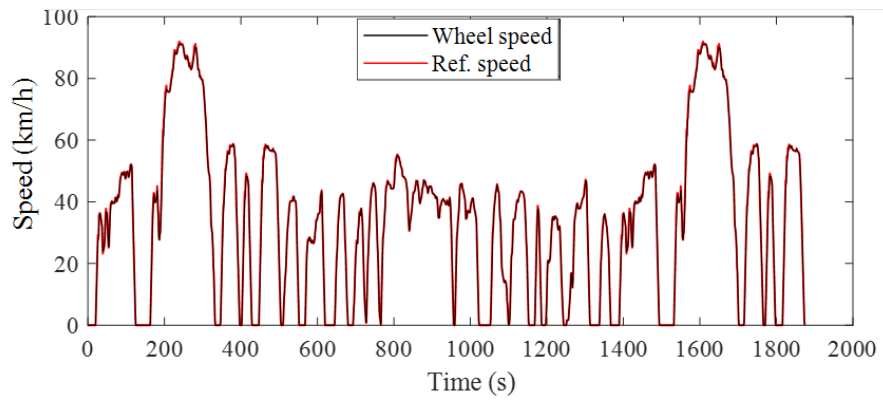


Fig. 4.11. Required motor operation points for UDDS.



(a)

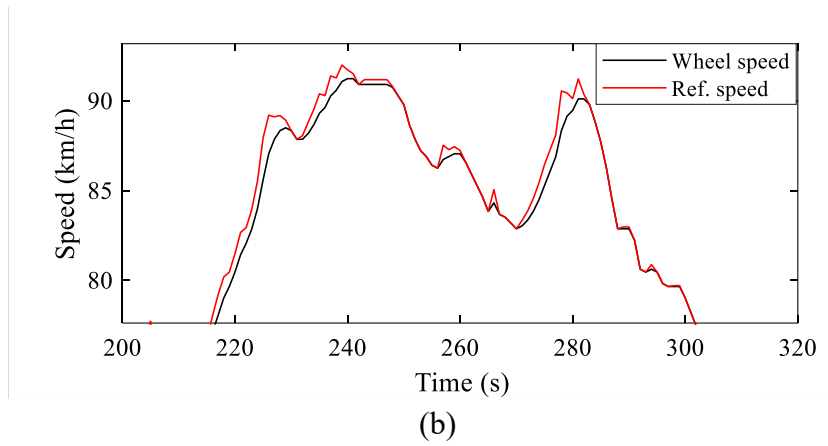


Fig. 4.12. UDDS reference speed vs wheel speed.

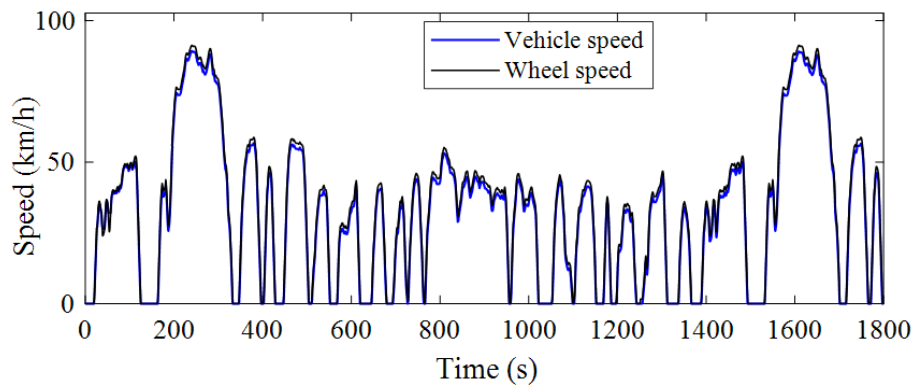


Fig. 4.13. Simulated vehicle speed and wheel speed for UDDS.

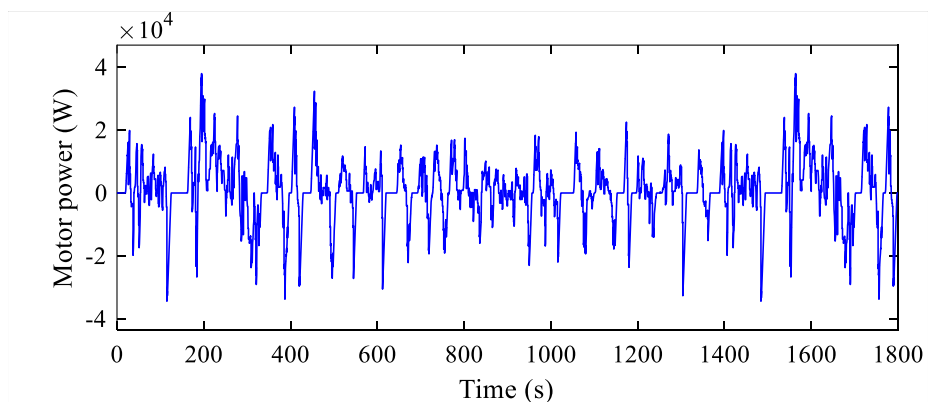


Fig. 4.14. The power of the PM motor under UDDS.

4.4.2 HWFET test under the dry concrete road condition

HWFET represents the highway driving conditions. The analysis of the PM motor based on HWFET under the dry concrete road condition is to identify the capability of the PM motor as traction for highway driving. Fig. 4.15 shows the required torque-speed operation points for HWFET driving condition. The main operation points gather around the PM motor speed region of 3000 rpm to 5000 rpm with rated torque region. From the information in Fig. 4.18, the PM motor operates in rated power realm. The simulated wheel speed can trace the reference speed, as shown in Fig. 4.16, which prove the PM motor can meet the highway driving requirement. The average speed of HWFET is 77.7 km/h. Since there is a sharp acceleration at the beginning of the HWFE and a small amount of wheel slip happened, the difference of the actual vehicle speed and the wheel speed is observable. The analysis of results indicates that the PM motor can meet the requirements of highway driving for EV application.

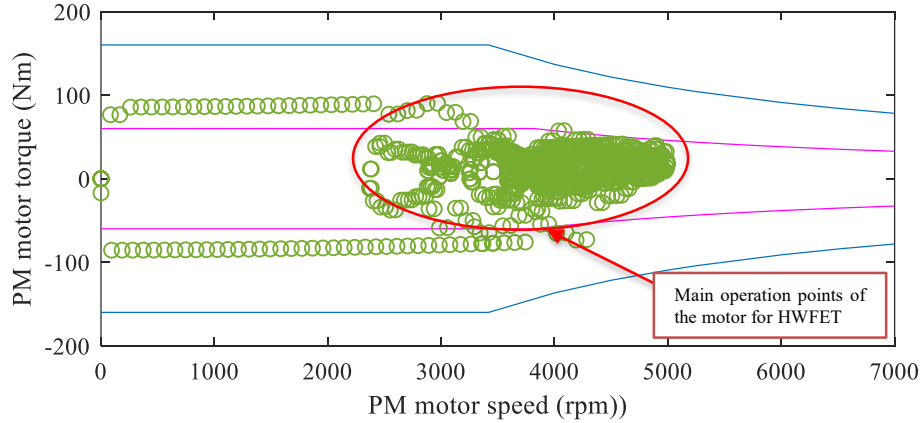


Fig. 4.15. Required motor operation points for HWFET

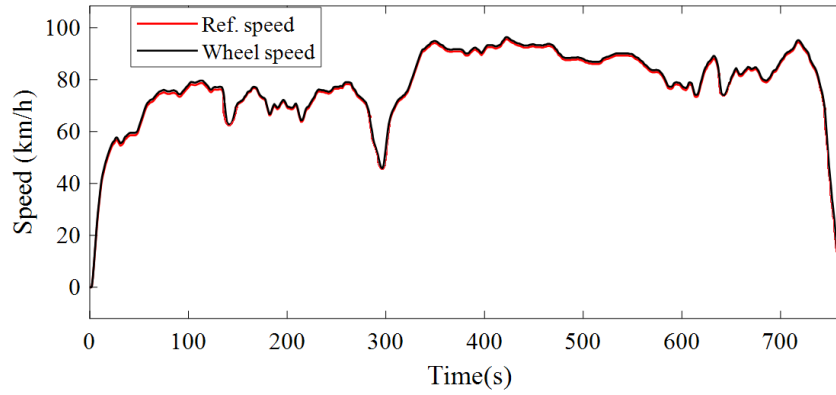


Fig. 4.16. HWFET reference speed vs wheel speed.

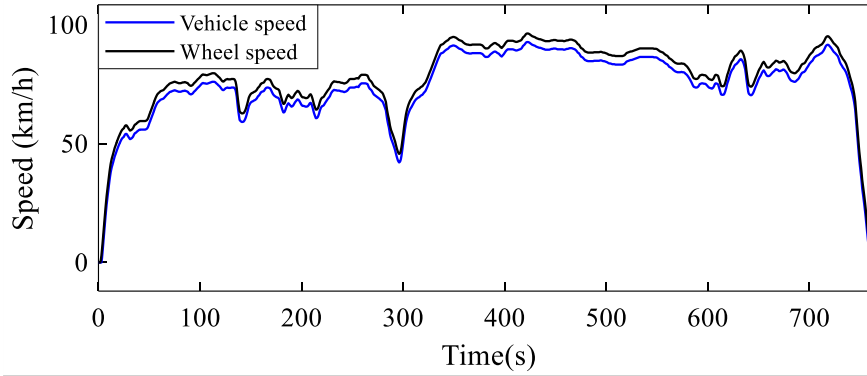


Fig. 4.17. Simulated vehicle speed and wheel speed for HWFET.

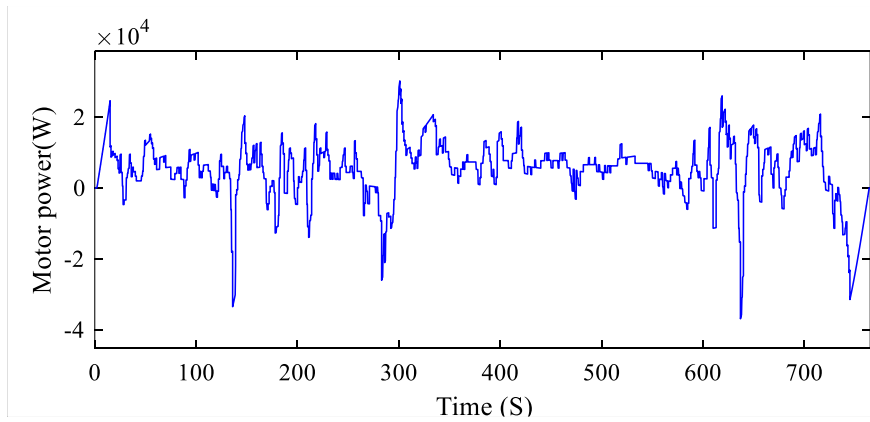


Fig. 4.18. The power of the PM motor under HWFET.

4.4.3 UDDS test under the snowy road condition

When the vehicle is driving on a snowy road surface, it is often accompanied by considerable wheel slippage, especially, when the driver gives sharp accelerating or braking. UDDS contains a certain amount of rapid acceleration and brake times. The driving behavior of the vehicle employing the PM motor under the snowy road condition is simulated. Fig. 4.19 shows the simulated vehicle speed and the reference speed of UDDS testing under the snowy road condition without slip control. In the proposed system, the test motor is in speed control mode and the feedback speed is the wheel speed instead of the vehicle speed. Additionally, the speed command to the tested motor and the torque command to the dyno motor are predefined and not vary with the actual simulated vehicle speed. When wheel slip happens, the vehicle speed will not keep track one reference speed with time. It will try to follow the predefined reference speeds for each time step. That is the reason why the vehicle speed has the same variation trend with the reference speed, which is not the reaction of the vehicle in practice. From the period of 0-850s, the simulated vehicle speed is smaller than the wheel speed because of high wheel slip ratio during the acceleration time. After the vehicle speed achieved the reference speed, the wheel speed is smaller than the vehicle due to the braking skidding. The detail of the wheel slip ratio without is shown in Fig. 4.20.

With the wheel slip control, the required motor torque is adjusted accordingly. The optimal wheel slip ratio is set as 0.12 according to empirical results of Magic formula model. Fig. 4.21 shows the adjusted torque applied to the wheels to use the maximum adhesion of the road. Fig. 4.21 (b) is the zoom in part of Fig. 4.21 (a). The torque delivered to the wheels is less than 50 Nm, which will cause less slip. Even with wheel slip control, the vehicle still can not achieve the reference for the whole driving cycle due to friction limitation of the snowy road. The speed tracking with the wheel slip control is shown in Fig. 4.22.

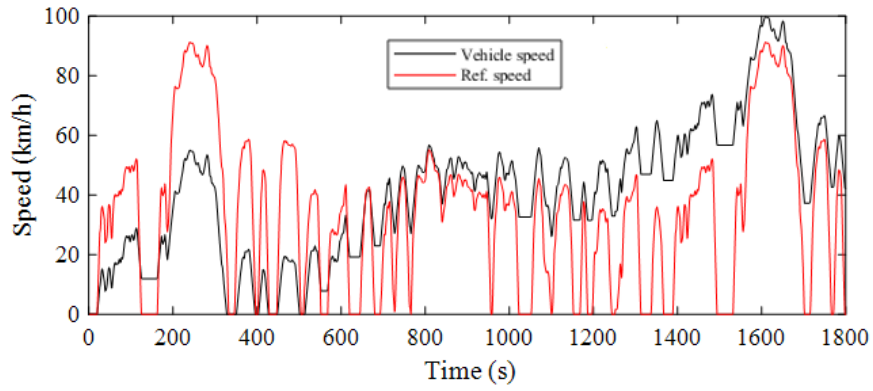


Fig. 4.19. Vehicle speed and reference speed without slip control.

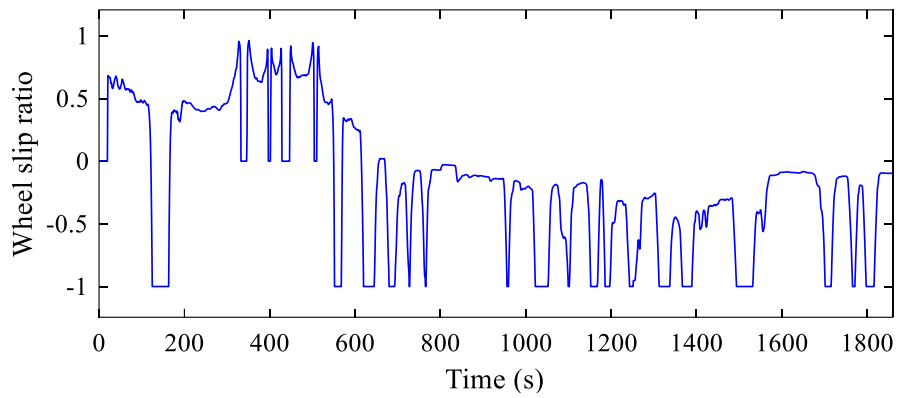
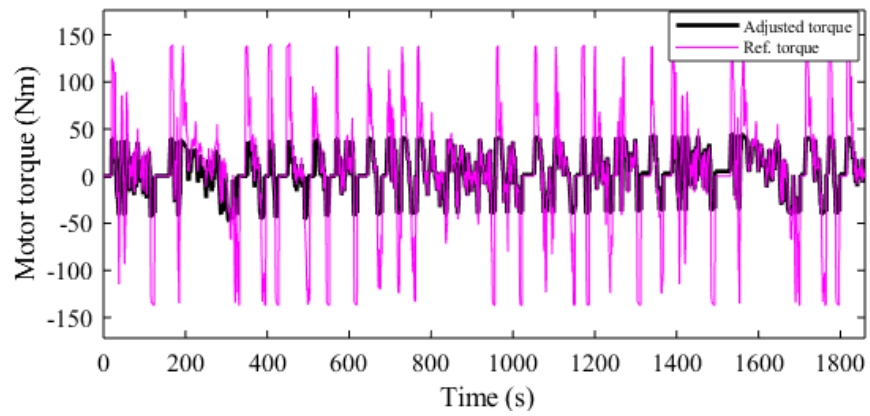
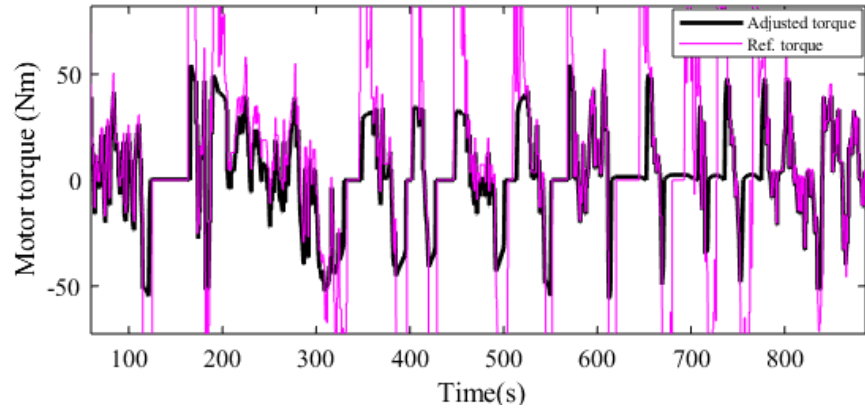


Fig. 4.20. Wheel slip ratio without slip control.



(a)



(b)

Fig. 4.21. Adjusted motor torque and reference motor torque.

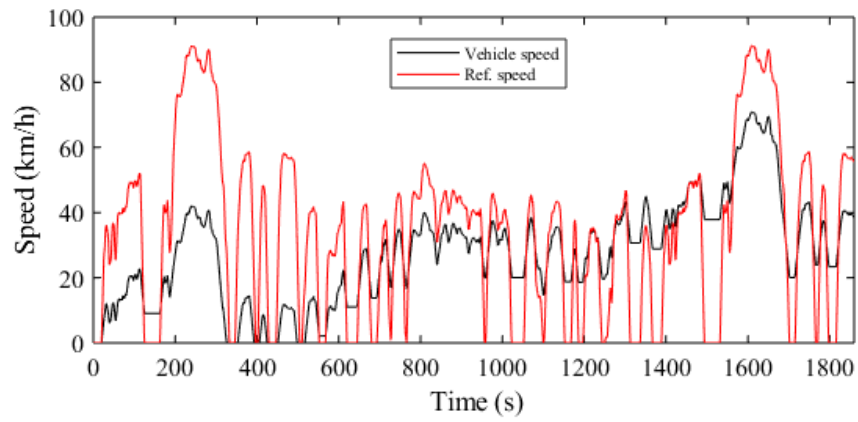


Fig. 4.22. Vehicle speed with slip control.

5 CONCLUSIONS AND FUTURE WORK

5.1 Conclusions

Electric vehicles are becoming more competitive than conventional vehicles driven by combustion engines in terms of improved energy efficiency and reduction in green house emission from the gas and developing high-performance electric motor drives, and battery packs are the most essential yet challenging steps for the advancement of electric vehicles. While battery packs depend highly on the innovation of materials, the traction motor drive has been one of the most interested research areas from both industry and academia due to the determinant role on the overall performance of the advanced vehicle such as improved reliability and extended driving range. To facilitate the electric vehicle development, comprehensive tests of the traction drive motor performed in realistic environments are highly demanded, especially at the preliminary stages of design and validation.

This work has been carried out to determine the candidates of traction motors and the corresponding performance evaluation through realistic tests. The main conclusions could be summarized as below.

- The analysis of electric motor requirements for EV application is conducted to determine the candidates as traction motors, and it is found the PM motors are more competitive than other types of motors. The investigation the torque-speed characteristics of electric motor shows that electric vehicles are more appealing than conventional vehicles in the aspect of dynamic performance.
- The testing of electric motors for EV application is quite different from that of industrial motors. Based on the literature on testing the electric motors as propulsion systems, a more specific testing method is proposed to mimic the application environment of the electric motors.

- A PMSM mathematical model is developed in the d-q coordinate system. The control strategy of PMSM for EV application is adopted using MTPA control and flux weakening control.
- Based on the forward/backward electric vehicle simulation, a vehicle dynamic model and a vehicle load model are constructed by considering the wheel slip.
- In order to accommodate vehicle slippery on roads, wheel slip control is integrated into the proposed testing environment. Five control algorithms of wheel slip control are analyzed, and comparisons are made, and fuzzy logic control is determined as the most suitable control method and is further applied for investigation.
- The PM motor is tested under UDDS & HWFET when the vehicle is running on dry concrete road respectively. The simulation results show the tested PM motor is capable of needs to city driving and highway driving. With the wheel slip control, the proposed testing environment are able to simulate the case of driving on the snowy road with the PM motor.

5.2 Future Work

The proposed PM motor testing environment towards EV application, featuring with wheel slip control, is a virtual electric vehicle operating environment for electric motor testing system. The final goal is to provide an innovative method of traction motor testing through the combination of both the software and hardware approaches. Implementation of this testing environment on the testing system will be done in the future by integrating driver module, vehicle dynamics, vehicle load and wheel slip control into the testing system.

REFERENCES

- [1] N. C. Kar, K. L. V. Iyer, A. Labak, X. Lu, C. Lai, A. Balamurali, B. Esteban and M. Sid-Ahmed, "Courting and Sparking: Wooing Consumers? Interest in the EV Market," *IEEE Electrification Magazine*, vol. 1, no. 2325-5897, pp. 21-31, Sept. 2013.
- [2] K. T. Chau and W. Li, "Overview of electric machines for electric and hybrid vehicles," *International Journal of Vehicle Design*, vol. 64, pp. 46-7, Sep. 2013.
- [3] M. Chang and C. C. Chan, *General Requirement of Traction Motor Drives*, John Wiley & Sons, Ltd., Apr. 2014.
- [4] M. Ehsani, Y. Gao and S. Gay, "Characterization of electric motor drives for traction applications," in *The 29th Annual Conference of the IEEE*, Roanoke, 2003.
- [5] E. F. Badin, *Hybrid vehicles from components to system*, Paris: IFP Energies nouvelles, 2013.
- [6] S. Beganović and S. Dacić, "Comparison of Dynamic Characteristics of Electric and Conventional Road Vehicles," in *Green Design Conference*, Netherlands, 2012.
- [7] Z. Yang, F. Shang, I. P. Brown and M. Krishnamurthy, "Comparative Study of Interior Permanent Magnet, Induction, and Switched Reluctance Motor Drives for EV and HEV Applications," *IEEE Transactions on Transportation Electrification*, vol. 1, no. 3, pp. 245 - 254, Oct. 2015.
- [8] G. Nanda and N. C. Kar, "A Survey and Comparison of Characteristics of Motor Drive Used in Electric Vehicles," in *Canadian Conference on Electrical and Computer Engineering*, Ottawa, 2006.
- [9] F. Richards, "<http://www.machinedesign.com>," 09 Apr. 2013. [Online]. Available: <http://www.machinedesign.com/motorsdrives/motors-efficiency-permanent-magnet-reluctance-and-induction-motors-compared>.
- [10] M. Hoyer, "<http://www.machinedesign.com>," Applications Engineer HBM Inc., 18 Nov. 2013. [Online]. Available:

<http://www.machinedesign.com/motorsdrives/misconceptions-ev-motor-testing>.

- [11] P. Fajri, V. A. K. Prabhala and M. Ferdowsi, "Emulating On-Road Operating Conditions for Electric-Drive Propulsion Systems," *IEEE Transactions. on Energy Conversion*, vol. 31, no. 1, pp. 1-11, March 2016.
- [12] C. M. A. E. D. W. Gao, "Modeling and Simulation of Electric and Hybrid Vehicles," *Pro. IEEE*, vol. 95, pp. 729-745, Apr. 2014.
- [13] J. Huo and X. Guo, "Modeling and Simulation of Hybrid Electric Vehicles using HEVSIM and ADVISOR," in *Proc. IEEE Veh. Power Prop. Conf.*, 2008.
- [14] A. Z. K. H. M. T. B. Ganji, "Drive Cycle Analysis of the Performance of Hybrid Electric Vehicles," *Life System Modeling and Intelligent Computing*, pp. 434-444, 2010.
- [15] J. J. Poon, M. A. Kinsy, N. A. Pallo, S. Devadas and I. L. Celanovic, "Hardware-in-the-Loop Testing for Electric Vehicle," in *Applied Power Electronics Conference and Exposition (APEC)*, Orlando, Feb. 2012.
- [16] S. G. Semenov, "Automation of Hardware-in-the-Loop and In-the-Vehicle Testing and Validation for Hybrid Electric Vehicles at Ford," *SAE Tech*, 2006.
- [17] X.-M. X., L.-F. X., B. H., X.-H. L. and M.-G. O., "Real Time Simulation of SHEV Powertrain system," *J. Syst. Simul*, vol. 16, pp. 1467-1471, 2004.
- [18] A. M. Lulhe and T. N. Date, "A Design & MATLAB Simulation of Motor Drive used for Electric Vehicle," in *IEEE ICCICCT*, Kumaracoil, 2015.
- [19] F. Zendri, R. Antonello, F. Biral and H. Fujimoto, "Modeling, identification and validation of an electric vehicle for model-based control design," in *IEEE International Workshop on Advanced Motion Control*, Nagaoka, March 2010.
- [20] R. Sehab and T. Shanan, "Control Laws for the Emulation of an Electric Vehicle Drivetrain by Two Electric Machines," in *IEEE Vehicle Power and Propulsion Conference (VPPC)*, Beijing, 2013.
- [21] P. Fajri, R. Ahmadi and M. Ferdowsi, "Control approach based on equivalent vehicle rotational inertia suitable for motor-dynamometer test bench emulation of electric vehicles," in *IEEE International Electric Machines & Drives Conference*, Chicago, 2013.

- [22] G. Park, SeonghunLee, S. Jinb and S. Kwakc, "Integrated modeling and analysis of dynamics for electric vehicle powertrains," *ELSEVIER Expert System with Application*, vol. 41, no. 5, pp. 2595-2607, April 2014.
- [23] M. Takeda, Y. Hosoyamada, N. Motoi and A. Kawamura, "Development of the experiment platform for electric vehicles by using motor test bench with the same environment as the actual vehicle," in *IEEE 13th International Workshop on Advanced Motion Control (AMC)*, Yokohama , 2014.
- [24] M. Kardaz and M. Kazerani, "System Electric Vehicle Scaling for Test Bed Simulation," in *IEEE Transportation Electrification Conference and Expo (ITEC)*, Dearborn, July 2016.
- [25] S. Mangan and J. Wang, "Development of a Novel Sensorless Longitudinal Road Gradient Estimation Method Based on Vehicle CAN Bus Data," *IEEE/ASME Transactions. on Mechatronics*, vol. 12, no. 3, pp. 375 - 386, 2007.
- [26] P. Pillay and R. Krishnan, "Modeling of permanent magnet motor drives," *IEEE Transactions on Industrial Electronics*, vol. 35, no. 4, pp. 537 - 541, 1988.
- [27] R. Krishnan, Permanent Magnet Synchronous and Brushless DC Motor Drives, Blacksburg, Virginia, U.S.A.: Taylor and Francis Group, LLC, 2010.
- [28] J. L. K. N. H.-B. I. a. H.-G. K. Gubae Kang, "A MTPA Control Scheme for an IPM Synchronous Motor Considering," in *IEEE Applied Power Electronics Conference and Exposition*, Kyungki-Do, Korea, 2004.
- [29] R. V. Chacko, M. L. Sreedevi and G. R. Mineeshma, "Electric vehicle power train simulation in forward modelling approach to enable real-time simulation and HIL controller prototyping," in *2014 IEEE International Conference on Power Electronics, Drives and Energy Systems (PEDES)*, Mumbai, India, 2014.
- [30] R. L. A. M. M. Federico, "Numerical Analysis for Vehicle Powertrian Development," in *Numerical Analysis- Theory and Application*, In Tech, 2011, pp. 519-540.
- [31] K. B. Wipke, M. R. Cuddy and S. D. Burch, "ADVISOR 2.1: a user-friendly advanced powertrain simulation using a combined backward/forward approach," *IEEE Transactions on Vehicular Technology*, vol. 48, no. 6, pp. 1751-1761, 1999.
- [32] T. Markel, A. Brooker, T. Hendricks, V. Johnson, K. Kelly, B. Kramer, M.O'Keefe,

- S. Sprik and K. Wipke, "ADVISOR: a systems analysis tool for advanced vehicle modeling," *ELSEVIER Journal of Power Sources*, vol. 110, no. 2, pp. 255-266, Aug. 2002.
- [33] T. D. Gillespie, in *Fundamentals Of Vehicle Dynamics*, Society of Automotive, 1992, pp. 1-19.
- [34] J. Y. Wong, in *Theory of Ground Vehicles*, John Wiley & Sons , Inc., 2008, p. 9.
- [35] M. Ehsani, Y. Gao and A. Emadi, in *Modern Electric, Hybrid Electric, and Fuel Cell Vehicles: Fundamentals, Theory, and Design*, USA, CRC Press, 2009, p. Chap. 2.
- [36] J. Taborek, *Mechanics of Vehicle*, Cleveland, Ohio: Penton Publishing Co., , 1957.
- [37] K. Reeves, A. Montazeri and C. J. Taylor, "Validation of a Hybrid Electric Vehicle dynamics model for energy management and vehicle stability control," in *IEEE 25th International Symposium on Industrial Electronics (ISIE)*, Santa Clara, 2016.
- [38] L. Bin, Y. Xiaobo and J. Yang, "Tire Model Application and Parameter Identification-A Literature Review," *SAE Int. J. Passeng. Cars – Mech. Sys*, p. 231–243, 2014.
- [39] L. Li, F.-Y. Wang and Q. Zhou, "Integrated longitudinal and lateral tire/road friction modeling and monitoring for vehicle motion control," *IEEE Transactions on Intelligent Transportation Systems*, vol. 7, no. 1, pp. 1-19, 2006.
- [40] H. B. Pacejka, "The Magic Formula Tyre Model," in *Tyre and Vehicle Dynamics*, Amsterdam ; Boston : Elsevier/BH, 2012, p. 165.
- [41] T. M. B. H. J. K. K. O. S. Wipke, "ADVISOR: a systems analysis tool for advanced vehicle modeling," *Journal of Power Sources*, vol. 110, no. 2, pp. 255-266, 2002.
- [42] R. N. Jazar, *Vehicle Dynamics, Theory and Applications*, Springer, 2007.
- [43] S. Savaresi and M. Tanelli, "Active Braking Control Systems Design for Vehicles," in *Springer-Verlag*, New York, 2010.
- [44] U. Kiencke and L. Nielsen, "Automotive Control Systems for Engine, Driveline and Vehicle," in *Springer-Verlag*, New York, 2005.

- [45] T.-x. Zheng and F.-l. Ma, "Automotive ABS control strategy based on logic threshold," *Journal of Traffic and Transportation Engineering*, vol. 10, no. 2, pp. 69-74, 2010.
- [46] H. Li, L. Li, L. He, M. Kang, J. Song, L. Yu and C. Wu, "PID Plus Fuzzy Logic Method for Torque Control in Traction Control System," *International Journal of Automotive Technology*, vol. 13, no. 3, pp. 441-450, Apr. 2012.
- [47] T. Nakakuki, T. Shen and K. Tamura, "Adaptive control approach to uncertain longitudinal tire slip in traction control of vehicles," *Asian Journal of Control*, vol. 10, no. 1, pp. 67-73, 2008.
- [48] H. Mirzaeinejad and M. Mirzaei, "A novel method for non-linear control of wheel slip in anti-lock braking systems," *Control Engineering Practice*, vol. 18, no. 8, pp. 918-926, 2010.
- [49] H. Gao, R. Yu, X. Bai and H. Chen, "Vehicle Traction Control Based on Optimal Slip Using Sliding Mode Controller," in *33rd Chinese Control Conference*, Nanjing, China, 2014.
- [50] M. Amodeo, A. Ferrara, R. Terzaghi and C. Vecchio, "Wheel Slip Control via Second-Order Sliding-Mode Generation," *IEEE Transactions on Intelligent Transportation Systems*, vol. 11, no. 1, pp. 122-131, 2010.
- [51] A. E. Hadri, J. Cadiou, K. M'Sirdi and Y. Delanne, "Wheel-Slip Regulation Based on Sliding Mode Approach," in *SAE Technical Paper*, 2001.
- [52] Y. Lee and S. H. Zak, "Designing a Genetic Neural Fuzzy Antilock-Brake-System Controller," *IEEE Transactions on Evolutionary Computation*, vol. 6, no. 2, pp. 198-211, 2002.
- [53] P. Khatun, C. M. Bingham, N. Schofield and P. H. Mellor, "Application of fuzzy control algorithms for electric vehicle antilock braking/traction control systems," *IEEE Transactions on Vehicular Technology*, vol. 52, no. 5, pp. 1356-1364, 2003.
- [54] C. Lin and C. Hsu, "Neural-Network Hybrid Control for Antilock Braking Systems," *IEEE Transactions on Neural Networks*, vol. 14, no. 2, pp. 351-359, 2003.
- [55] A. Haddoun, M. E. H. Benbouzid, D. Diallo, R. Abdessemed, J. Ghouili and K. Srairi, "Analysis, Modeling and Neural Network Traction Control of an Electric Vehicle without Differential Gears," in *IEEE International Electric Machines &*

Drives Conference, Antalya, Turkey, 2007.

- [56] V. I. Utkin, "Variable Structure systems with Sliding Modes," *IEEE Trans.* , vol. 22, no. 2, pp. 212-222, 1977.
- [57] A. A. Ahmeda, R. Ahmadb, A. Yahya, H. H. Tahir and J. Quinlan, "Variable Structure System with Sliding Mode Controller," *Procedia Engineering*, pp. 441-452, 2013.
- [58] C. C. Lee, "Fuzzy logic in control systems: fuzzy logic controller," *IEEE Transactions on Systems, Man, and Cybernetics*, vol. 20, no. 2, pp. 404-418, 1990.
- [59] G. F. Mauer, "A fuzzy logic controller for an ABS braking system," *IEEE Transactions on Fuzzy Systems*, vol. 3, no. 4, pp. 381 - 388, 1995.
- [60] G. Wang, Z. Liu and R. Hu, "Fuzzy logic direct adaptive control of ABS-equipped vehicle based on equivalent slip differential of tire," *Chinese Journal of Mechanical Engineering*, vol. 44, no. 11, pp. 242-247, 2008.
- [61] F. Tahami, R. Kazemi, S. Farhanghi and B. Samadi, "Fuzzy Based Stability Enhancement System for a Four-Motor-Wheel Electric Vehicle," in *SAE, Automotive Dynamic & Stability*, 2002.
- [62] C. Canudas-de-Wit, P. Tsiotras, E. Velenis, M. Basset and G. Gissinger, "Dynamic Friction Models for Road/Tire Longitudinal Interaction," in *Vehicle System Dynamics*, Taylor & Francis Group, 2003, pp. 189-226.
- [63] W. V. Leekwijck and E. E. Kerre, "Defuzzification: criteria and classification," *Fuzzy Sets and Systems*, vol. 108, no. 2, pp. 159-178, 1999.

LIST OF PUBLICATIONS

- [1] Q. Xie, C. Filho, G. Feng, W. Clandfield, and N. Kar, “Advanced Vehicle Dynamic Model for EV Emulation Considering Environment Conditions”, *IEEE CCECE*, May 2017.
- [2] Q. Xie, E. Zhu, J. Tjong, and N. C. Kar, “Acoustic Noise Based Permanent Magnet Flux Reduction Diagnosis and Current Compensation in PMSM,” *IEEE InterMag*, Ireland, April 2017.

APPENDIX

I: Permanent magnet synchronous machine parameters:

Rated voltage	275 V
Rated current	64 A
Rated power	24 kW
Peak power	57.2 kW
Rated speed	3880 rpm
Peak speed	7000 rpm
Rated torque	60 Nm
Peak torque	160 Nm
d-inductance	0.376 mH
q-inductance	0.232 mH
Magnet flux linkage	0.15
Back-EMF coefficient	62.5 V/krpm
Nominal power	50 hp
No. of poles	4
Stator resistance (R_s)	0.087 Ω
Mutual inductance (L_m)	34.7x10 ⁻³ H
Inertia constant (H)	1.662 kg-m ²

II: Target vehicle configuration and related parameters:

Mass of the vehicle	1500 kg
Vehicle frontal area	2.15 m ²
Aerodynamics coefficient	0.315
Gravity	9.8m/s ²
Gear ratio	6.25
Wheel effective radius	0.3083m
Wheel inertia	0.089 kgm ²
Rolling resistance coefficient (dry concrete)	0.011
Efficiency of driveline	0.93
Gear box inertia	0.5kgm ²
Height of the gravity (CG)	0.634 m
Distance between the base of the two wheels	2.65 m
Distance between CG and the front wheel base	1.13m
Distance between CG and the rear wheel base	1.52 m
Front weight	57.3%
Rear weight	42.7%
Mass density of air	1.202 kg/m ³

VITA AUCTORIS

Name Qingqing Xie

Place of Birth Chongqing, China

Education *University of Windsor, Windsor, Ontario, Canada*
2016 - 2018
M.A.Sc.

University of Windsor, Windsor, Ontario, Canada
2015 - 2016
M.eng.

University of East China Jiaotong, Jiangxi, China
2007 - 2011
B.Sc.